



1 **Spatial-temporal changes in flow hydraulic characteristics and soil loss**
2 **during gully headcut erosion**

3

4 Mingming Guo^a, Zhuoxin Chen^b, Wenlong Wang^{b,c*}, Tianchao Wang^d, Qianhua Shi^b, Hongliang

5 Kang^b, Man Zhao^b, Lanqian Feng^c

6

7 a Key laboratory of Mollisols Agroecology, Northeast Institute of Geography and Agroecology,

8 Chinese Academy of Sciences, Harbin 150081, Heilongjiang, China

9 b State Key Laboratory of Soil Erosion and Dryland Farming on the Loess Plateau, Institute of Water
10 and Soil Conservation, Northwest A&F University, Yangling, Shaanxi 712100, China

11 c Institute of Soil and Water Conservation, Chinese Academy of Sciences and Ministry of Water
12 Resources, Yangling, Shaanxi 712100, China

13 d Ulanyab Grassland Station, Jining, Inner Mongolia 012000, China

14 ***Corresponding author:** Wenlong Wang

15 E-mail addresses: nwafu_wwl@163.com; wllwang@nwsuaf.edu.cn

16



17 **Abstract**

18 The temporal-spatial changes in flow hydraulics and energy consumption and their associated soil
19 erosion remain unclear during gully headcut retreat. A simulated scouring experiment was conducted
20 on five headcut plots consisting of upstream area (UA), gully headwall (GH) and gully bed (GB) to
21 elucidate the temporal-spatial changes in flow hydraulic, energy consumption, and soil loss during
22 headcut erosion. The flow velocity at the brink of headcut increased as a power function of time,
23 whereas the jet velocity entry to plunge pool and jet shear stress logarithmically or linearly decreased
24 over time. The jet properties significantly affected by upstream flow discharge. The Reynold number,
25 runoff shear stress, and stream power of UA and GB increased as logarithmic or power functions of
26 time, but the Froude number decreased logarithmically over time. The flow of UA and GB was
27 supercritical and subcritical, respectively, and transformed to turbulent with inflow discharge
28 increased. The Reynold number, shear stress and stream power decreased by 56.0%, 63.8% and
29 55.9%, respectively, but the Froude number increased by 7.9% when flow dropped from UA to GB.
30 The accumulated runoff energy consumption of UA, GH and GB positions linearly increased with
31 time, and their proportions of energy consumption are 18.3%, 77.7% and 4.0%, respectively. The soil
32 loss rate of the “UA-GH-GB” system initially rose and then gradually declined and levelled off. The
33 soil loss of UA and GH decreased logarithmically over time, whereas the GB was mainly
34 characterized by sediment deposition. The proportion of soil loss at UA and GH are 11.5% and
35 88.5%, respectively, of which the proportion of deposited sediment on GB reached 3.8%. The change
36 in soil loss of UA, GH and GB was significantly affected by flow hydraulic and jet properties. The
37 critical energy consumption initiating soil erosion of UA, GH, and GB are 1.62 J s^{-1} , 5.79 J s^{-1} and
38 1.64 J s^{-1} , respectively. These results are helpful to reveal the mechanism of gully headcut erosion
39 and built headcut migration model.

40
41 **Keywords:** Gully erosion; Hydraulic property; Headcut retreat; Bank collapse; Loess Plateau

42



43 **1 Introduction**

44 Gully erosion is a typical soil erosion process whereby concentrated runoff from an upstream
45 drainage area recurs in a channel and erodes soil from the area through which runoff passed to
46 considerable depth (Poesen et al., 2003; Zhu, 2012). Gully erosion is recognized as the main
47 sediment source in some hilly and gully-dominated watersheds (Poesen et al., 2003; Valentin et al.,
48 2005; Dotterweich et al., 2012). Poesen et al. (2003) reported that soil loss amount caused by gully
49 erosion accounts for 10% - 94% of total soil loss amount based on the collected data from published
50 articles. Moreover, gully erosion can severely damage to infrastructure, enhance the terrain
51 fragmentation, and cause ecosystem instability, land degradation and food safety (Poesen et al., 2003;
52 de Vente & Poesen, 2005; Li et al., 2015; Vanmaercke et al, 2016; Hosseinalizadeh et al., 2019).

53 As one of the gully erosion processes, the gully headcut retreat often significantly influences
54 and determines gully erosion (Oostwoud-Wijdenes et al., 2000; Vandekerckhove et al., 2003; Guo et
55 al., 2019). A headcut is defined as a vertical or near-vertical drop or discontinuity on the bed of a
56 gully occurring where flow is concentrated at a knickpoint (Hanson et al., 2001; Bennett et al., 2000).
57 Many studies have demonstrated that the gully erosion is the result of the combined actions of plunge
58 pool erosion by jet flow, upstream runoff incision, headwall erosion by on-wall flow, mass failure
59 (gully head and wall collapse), (Vanmaercke et al., 2016; Addisie et al., 2017; Guo et al., 2019).
60 Once a headcut is formed in upstream area, the gully will develop rapidly and not stop forward until
61 a critical topographic condition is formed ($S \leq a \cdot A^b$, where S and A is the slope gradient and drainage
62 area upstream gully headcut, respectively) (Kirkby et al., 2003). Moreover, in fact, the erosion
63 processes of different landform units (upstream area, UA; gully head, GH; gully bed, GB) are
64 completely different during gully headcut erosion (Zhang et al., 2018; Guo et al., 2019; Shi et al.,
65 2020a). The combination and interaction of erosion processes of the three landform units determined
66 gully headcut erosion process (Vanmaercke et al., 2016). Therefore, clarifying the soil erosion
67 process and characteristics of the three landform units is critical to systematically and clearly reveal
68 the mechanism of gully headcut erosion.

69 Previous studies suggested that gully heacut erosion is affected by various factors including
70 topography, land use change, vegetation, soil properties, and climate (Vanwallegem et al., 2003;



71 Ionita, 2006; Rodzik et al., 2009; Rieke-Zapp and Nichols, 2011; Torri and Poesen, 2014; Ionita et al.,
72 2015; Vannoppen et al., 2015; Guo et al., 2019, 2020a). In terms of topography, most of studies
73 focused on the threshold relationship ($S \leq a \cdot A^b$) to initiate gully erosion (e.g. Torri and Poesen, 2014).
74 Several experimental studies demonstrated that the upstream slope gradient and headcut height have
75 significant effects on headcut erosion (e.g. Bennett, 1999; Zhang et al., 2018). Land use change is
76 recognized as having the strongest effect on processes related to gully erosion among influencing
77 factors (Poesen et al., 2003; Chaplot et al., 2005; Descroix et al., 2008), and also significantly affects
78 the activation of gully headcut erosion (e.g. Torri and Poesen, 2014). In this aspect, the vegetation
79 coverage is a parameter that is often used to clarify its effect on gully erosion (e.g. De Baets et al.,
80 2007; Martínez-Casasnovas et al., 2009), however, in fact, the vegetation effect mainly depended on
81 the root characteristics and its distribution at gully head (e.g. Vannoppen et al., 2015; Guo et al.,
82 2019). Nevertheless, at present, the most of studies on gully erosion focus on the changes in gully
83 morphology between different periods at a watershed or regional scale (Vanmaercke et al., 2016),
84 which is why the previous studies fail to address the effects of root systems on gully headcut retreat.
85 Guo et al. (2019) concluded that the grass (*Agropyron cristatum*) could reduce soil loss and headcut
86 retreat distance by 45.6–68.5%, 66.9–85.4%, respectively, and the roots of 0–0.5 mm in diameter
87 showed the greatest controlling influence on headcut erosion. In terms of soil properties, lots of
88 studies have proved the significant effect of soil properties on gully headcut erosion (e.g. Nazari
89 Samani et al., 2010), which was mainly related to the change in soil erodibility induced by soil
90 properties including soil texture, soil vertical joints, soluble mineral content, soil lithology, and
91 physicochemical properties (Sanchis et al., 2008; Vanmaercke et al., 2016; Guo et al., 2020a).
92 Rainfall, the main climate factor, is closely related to runoff generation and thus be expected to affect
93 headcut erosion. Many studies have reported that the initiation of gully headcut is correlated with
94 rainfall characteristics (e.g. summation of rainfall from 24-hour rains equal to or greater than 0.5
95 inches) (Beer and Johnson, 1963; Vandekerckhove et al., 2003; Rieke-Zapp and Nichols, 2011).
96 However, the great difference in the threshold value relating to rainfall factors was found among
97 different areas of the world due to great difference in erosion environment. For example, in the
98 northeast of China, the gully erosion is the result of soil thawing, rainfall runoff and snowmelt runoff



99 (Li et al., 2016b; Xu et al., 2019). Furthermore, at present, the most of studies on gully erosion were
100 conducted to quantify the change in gully erosion (retreat rate, area and volume) at different spatial
101 and temporal scales by using remote sensing interpretation, real-time monitoring and meta-analysis
102 based on literature data (e.g. Vanmaercke et al., 2016). However, the influencing mechanism of these
103 factors on gully headcut erosion is still unclear and need to be revealed in future studies.

104 Evidently, the concentrated flow upstream gully head, mainly depended on the upstream area
105 and rainfall, is the main and original drive force triggering headcut erosion. The runoff firstly eroded
106 the upstream area and then was parted into two types of flow (on-wall flow and jet flow) at the
107 brinkpoint of gully headcut. Consequently, the on-wall flow persistently eroded the headwall soil,
108 and the jet flow violently impacted gully bed soil and formed a plunge pool (Su et al., 2015; Guo et
109 al., 2019). Subsequently, the two types of flow merged again and eroded gully bed together (Zhang et
110 al., 2018; Shi et al., 2020a). The runoff hydraulic or jet flow properties at different landform units
111 (upstream area, gully head and gully bed) are significantly different, which is an important reason for
112 the difference in erosion process among different landform units. However, the temporal-spatial
113 change in runoff and jet properties during headcut erosion is still unclear and thus needs to be
114 clarified. Furthermore, at present, some experimental studies on headcut erosion of rill, ephemeral
115 gully, gully and bank gully were conducted to investigate the runoff properties, energy consumption,
116 sediment transport process, morphology evolution and empirical model (Bennett and Casali, 2001;
117 Wells et al., 2009a, 2009b; Su et al., 2014; Xu et al., 2017a; Guo et al., 2019; Shi et al., 2020a).
118 However, relatively few knowledges were obtained to systemically reveal the hydrodynamic
119 mechanism of gully headcut erosion. Therefore, elucidating the temporal-spatial changes in runoff
120 hydraulic and soil loss and hydrodynamic mechanism of UA, GH and GB is of great importance to
121 systematically reveal the hydrodynamics mechanism of gully headcut erosion.

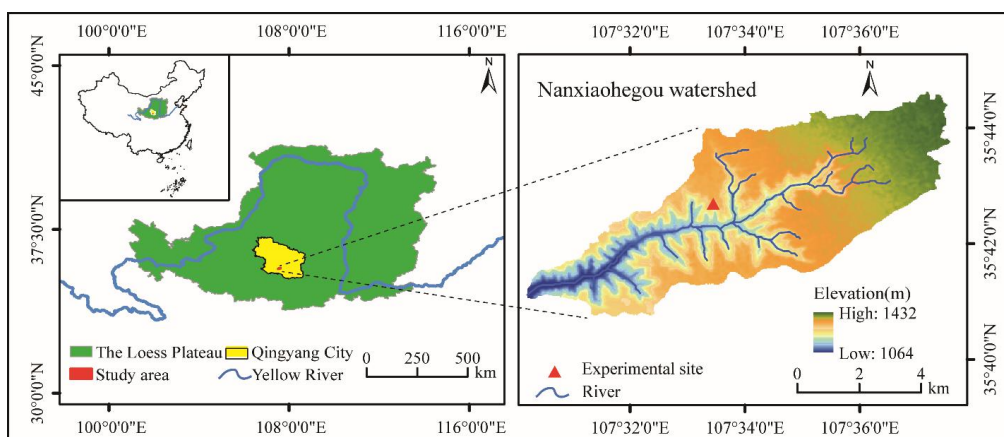
122 Given the above-mentioned issues, a series of simulated gully headcut erosion experiments
123 subjected to inflow scouring are conducted to (1) investigate the temporal-spatial change in hydraulic
124 properties and soil loss during headcut erosion, (2) quantify the energy consumption and soil loss
125 distribution of UA, GH and GB, and (3) reveal the erosion hydrodynamic mechanism of UA, GH
126 and GB.



127 **2 Materials and Methods**

128 **2.1 Study area**

129 This experiment was carried out at the Xifeng Soil and Water Conservation Experimental
130 Station that is located in the Nanxiaohegou watershed, Qingyang City, Gansu Province, China (Fig.
131 1). The study area belongs to a semi-arid continental climate with a mean annual temperature of
132 9.3 °C. The mean annual precipitation is 546.8 mm (1954 - 2014), of which precipitation from May
133 to September accounts for 76.9% of the total precipitation. The elevation ranges from 1050 to 1423
134 m (Xia et al., 2017; Guo et al., 2019). The main landforms include gentle loess-tableland, steep
135 hillslope and gully channel, and their areas account for 57.0%, 15.7% and 27.3%, respectively. The
136 loess-tableland is characterized by low slope (1–5°), gentle and flat terrain and fertile soil. The main
137 soil type is loessial soil with silt loam texture. Most of hillslopes have been constructed as
138 slope-terraces. The main gully channel is usually U-shaped and the branch-gully is more actively
139 developed and easily eroded as a V-shaped by runoff from loess-tableland (Xu et al., 2019). The flat
140 loess-tableland can accumulate the 67.4% of total runoff and cause serious gully erosion that can
141 contribute 86.3% of the total soil erosion (Guo et al., 2019). The original plant species have been
142 seriously destroyed. Since the 1970s, the “Three Protection Belts” system, the “Four
143 Eco-Economical Belts” system and the “Grain for Green” project (Zhao, 1994; Fu et al., 2011) were
144 implemented to control soil erosion. The current mean annual soil erosion rate has been reduced to
145 4350 t km⁻² y⁻¹ in the study watershed (Guo et al., 2019). The previous vegetation are mainly
146 artificially planted forests and some native secondary herbaceous communities.



147

148 **Figure 1** The location of the experimental site in Nanxiaohegou watershed, Qingyang City, Loess
149 Plateau, China. Note: The figure production was based on the digital elevation model data (spatial
150 resolution of 30 m) which is available from <http://srtm.csi.cgiar.org> (Reuter et al., 2007).

151

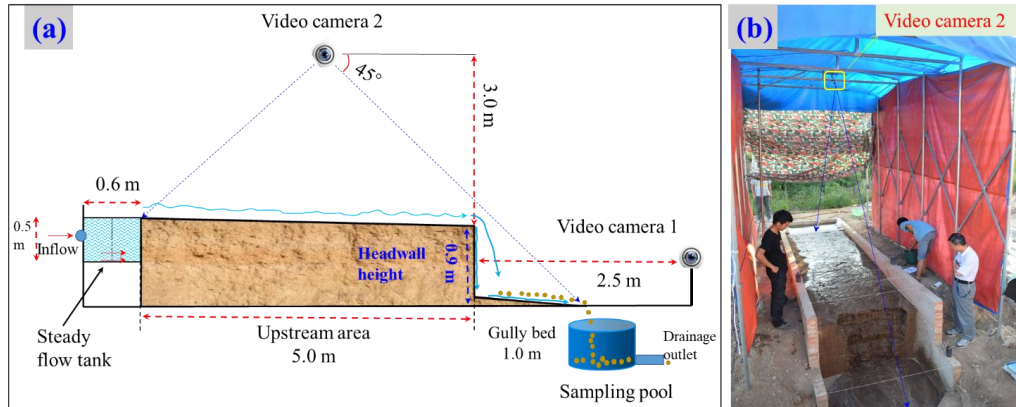
152 2.2 Experimental design

153 2.2.1 Gully head experimental plot construction

154 Five gully head plots for headcut erosion experiments were constructed at the experimental
155 station in April 2018. Fig. 2 shows the basic information of the gully head plot consisting of three
156 landform units (upstream area, headwall and gully bed). The plot width and slope gradient of
157 upstream area and gully bed are uniformly designed as 1.5 m and 3°, respectively. The upstream area
158 length, the height of the vertical headwall and the length of the gully bed are 5.0 m long, 0.9 m, and
159 1.0 m, respectively (Fig. 2a). The plot boundary was constructed in strict accordance with designed
160 plot dimension using cement and bricks (Fig. 2b). After the construction of plot boundary, the soil
161 was sieved through a 2 cm sieve with to remove roots and debris and ensure uniform soil underlying
162 condition. The sieved soil was filled into the plot every 10-cm thick layer according to the
163 investigated soil bulk density of gully heads. The soil surface of each layer was harrowed to increase
164 the cohesion between two soil layers (Guo et al., 2019). In general, the filling upstream area length
165 was 5.5 m that was larger than the precise upstream area length (5.0 m). After establishment of gully
166 head plots, the five plots were carefully managed about four months (August 2018) to allow the soil
167 to return to its natural state. During the four-month conservation process, the naturally growing
168 weeds were weeded out in time. Moreover, a flow-steady tank of 0.6 m, 1.5 m and 0.5 m in length,



169 width and height was installed at the top of upstream area, and a circular sampling pool of 0.6 m in
 170 diameter was set at the bottom of the gully bed to collect runoff and sediment (Fig. 2a).



171
 172 **Figure 2** Sketch (a) and photo (b) of experimental plot.
 173

174 2.2.2 Inflow discharge design

175 The concentrated runoff generated from upstream area is the main force driving gully headcut
 176 erosion. Jiao et al (1999) concluded that the more serious soil erosion is generally caused by “A”
 177 type rainstorm with the rainfall duration of 25 to 178 mins than other types of rainstorms in the Loess
 178 Plateau. Thus, an extreme case of rainfall duration (180 min) was considered in this study, and the
 179 recurrence period of “A” type rainstorm was designed as 30 years. Previous studies indicated that the
 180 rainstorm distribution on the Loess Plateau showed a non-significant change in past decades (Li et al.,
 181 2010; Sun et al., 2016; Wen et al., 2017). Zhang et al. (1983) proposed a statistical equation (Eq. (1))
 182 for calculating the average rainfall intensity by analyzing 1710 typical rainstorm events in the Loess
 183 Plateau. Then, the inflow discharge was calculated by Eq. (2) and ranged from 3.12 to 9.68 m³ h⁻¹.
 184 Considering the pre-experiment effect, finally, we selected the five inflow discharge levels (3.0, 3.6,
 185 4.8, 6.0, and 7.2 m³ h⁻¹).

$$186 \quad RI = \frac{5.09N^{0.379}}{(t+1.4)^{0.74}} \quad (1)$$

187 where RI is the average rainfall intensity during t minutes, mm min⁻¹; N is the recurrence period
 188 of rainstorm, yr; and t is the rainfall duration, min.

$$189 \quad q = \frac{60\alpha \cdot A \cdot RI \cdot w}{W} \quad (2)$$



190 where A is the upstream area (km^2) and has a wide range of 0.15 - 8.7 km^2 according to an early
191 investigation of research team (Che, 2012); W is the width of the upstream area, km; w is the plot
192 width, m; and α is the runoff coefficient of bare land and is identified as 0.167 by analyzing the
193 runoff and rainfall data of standard runoff plots (Li et al., 2006).

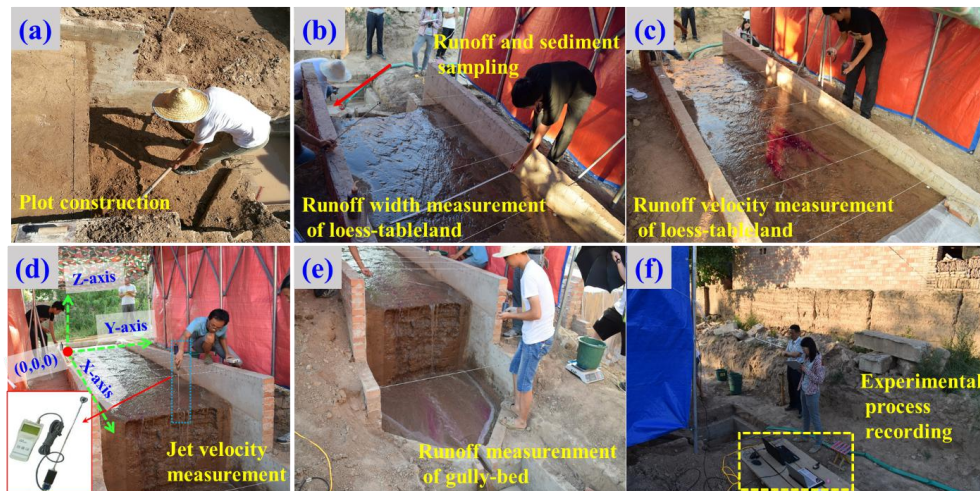
194 **2.3 Experimental procedure**

195 The scouring experiment was conducted in August 2018. Before formal experiment, firstly, the
196 upstream area length was adjusted to designed length of 5.0 m (Fig. 3a). Then, a self-made tent
197 (length \times width \times height: 6.0 m \times 3.0 m \times 3.5 m) with waterproof canvas enclosed the plot to resist
198 the effect of natural rainfall and sunshine on experimental progress and photo shooting for 3D
199 reconstruction (Fig. 2b). In addition, the experimental process was recorded by two Logitech 930e
200 video cameras with a resolution of 2.0 megapixels. The camera 1 was installed 2.5 m in front of plot
201 headwall (Fig. 2a), and the camera 2 was installed 3.0 m above the plot center (Fig. 2a).

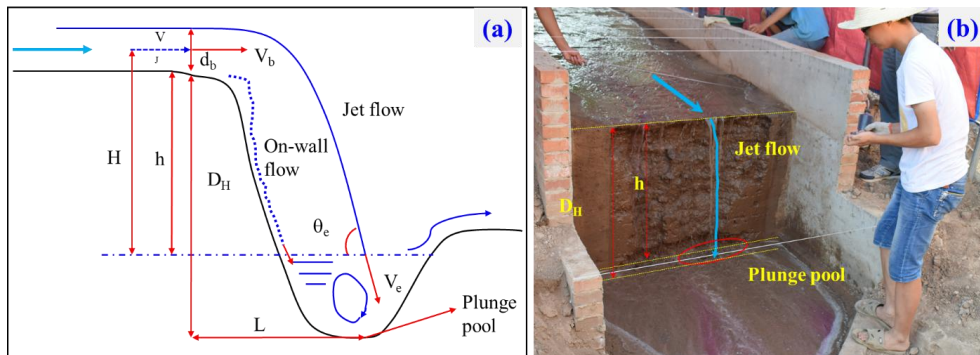
202 Before the experiment, watering can be used to spray each experimental plot until surface runoff
203 was generated, and then the plot was placed for 24 hours to ensure adequate water infiltration, which
204 can assure that the soil moisture of the five plots was approximately the same. The inlet pipeline was
205 placed in steady flow tank when the inflow discharge was adjusted to designed value. A water
206 thermometer was placed into the steady flow tank to monitor the change in water temperature during
207 experimental process. The runoff and sediment samples at the plot outlet were collected at 2-min
208 intervals to represent the temporal change in runoff and sediment of “UA – GH – GB” system, and
209 the sampling time was also recorded using a stopwatch (Fig. 3b). The runoff and sediment samples
210 were oven-dried at 105 °C for 24 h and weighed to calculate the soil loss rate of the “UA – GH – GB”
211 system (g s^{-1}). Besides, the timing of the collapse events was also recorded during headcut erosion.
212 The upstream area was divided into 4 runoff observation sections, and the runoff width (w), depth (d)
213 and velocity (V) of each section were measured by a calibrated scale of 1 mm accuracy and color
214 tracer method (Fig. 3b, 3c). The runoff velocity (V_r) before runoff arrived at the brink of headcut was
215 measured 5 – 8 times by the velocity measuring instrument (LS300-A) with the accuracy of 0.01 m
216 s^{-1} , and the runoff width at the headcut brinkpoint was measured (Fig. 3d). The runoff width and
217 velocity of gully bed were also measured using the same method with upstream area (Fig. 3e). Above



218 mentioned measurements of runoff characteristics and sediment samples were finished in 2-min
 219 intervals. The whole experimental process was recorded by two video cameras and imported into
 220 computers (Fig. 3f). In addition to above runoff parameters, the runoff depth (d_b) at the brink of
 221 headcut, the plunge pool depth (D_H) and the vertical distance (h) from brink-point of headcut to
 222 water surface of plunge pool were also measured 3 - 5 times by a steel ruler with 1 mm accuracy
 223 within each 2-min intervals (Fig. 4).



224
 225 **Figure 3** Runoff and sediment observation and recoding at upstream area, gully head and gully bed.



226
 227 **Figure 4** Sketch of jet flow at gully headcut and plunge pool at gully bed.

228



229 To obtain the temporal change in morphological characteristics during gully headcut erosion,
230 the experimental duration (180 min) was divided into six stage (30 – 60 – 90 – 120 – 150 – 180 min).
231 Photo-based three-dimensional (3D) reconstruction method was employed to obtain the digital
232 elevation model data of each plot prior to experiment and after each 30-min test. 14 target points
233 were placed around the plot for identifying the 3D coordinate before the photos were taken. The
234 eroded photographic was recorded by a Nikon D5300 camera with the focal length of 50 mm. The
235 following aspects were required during photos shooting: (1) obvious water on soil surface and direct
236 sunshine should be avoided, (2) a minimum overlap of 60% between subsequent photographs was
237 required, and (3) some complex eroded photographic should be taken in detail. In this study, the
238 upper left corner of the plot was set as the original coordinates (0, 0, 0) , and the direction of
239 three-dimensional coordinate was determined as shown in Fig. 3d. These collected photos were
240 imported in Agisoft PhotoScan software (Agisoft LLC, Russia, professional version 1.1.6), and then
241 these control points and their coordinates would be identified and entered. The root mean square
242 errors of the target points are 0.0037, 0.0045, 0.0024, 0.0052 and 0.0030 m on average, respectively,
243 for the experiments of five inflow discharges, which can satisfy the study requirement (millimeter
244 level). The DEM could be exported and was used to extract the morphological parameters and soil
245 loss volume of three landform units at six stages (Frankl et al., 2015).

246 **2.4 Parameter calculation, data analysis and figure plotting**

247 **2.4.1 Hydraulic parameters of upstream area and gully bed**

248 Five parameters including runoff velocity (V , m s⁻¹), Reynold number (Re), Froude number (Fr),
249 shear stress (τ , Pa) and stream power (ω , W m⁻²) were used to characterize the changes in hydraulic
250 properties at upstream area and gully bed positions. The five parameters are calculated as follows.

$$251 \quad Re = \frac{V \cdot R}{\nu} \quad (1)$$

$$252 \quad Fr = \frac{V}{\sqrt{g \cdot R}} \quad (2)$$

$$253 \quad R = \frac{w \cdot d}{w+2d}, \nu = \frac{1.775 \times 10^{-6}}{1+0.0337T+0.000221T^2} \quad (3)$$

$$254 \quad \tau = \rho_w \cdot g \cdot R \cdot J \quad (4)$$



255
$$\omega = \tau \cdot V \quad (5)$$

256 where R (m) and ν ($\text{m}^2 \text{s}^{-1}$) are the hydraulic radius and the water kinematic viscosity coefficient,
 257 respectively; w (m), d (m) and T ($^{\circ}\text{C}$) are the runoff width, depth and water temperature, respectively;
 258 ρ_w (kg m^{-3}) is the water density and J (m m^{-1}) is the hydraulic gradient.

259 2.4.2 Jet properties of gully head

260 Based on the measured runoff velocity (V_J , m s^{-1}) before runoff arrived at the headcut brinkpoint,
 261 the runoff depth (d_b , m) at the headcut brinkpoint, the plunge pool depth (D_H , m) and the vertical
 262 distance (h , m) (Fig. 4a), the three parameters including the runoff velocity at the headcut brinkpoint
 263 (V_b), jet-flow velocity entry to plunge pool (V_e) and jet-flow shear stress (τ_j) were calculated to
 264 clarify the change of jet properties (Rouse, 1950; Hager, 1983; Stein et al., 1993; Flores-Cervantes et
 265 al., 2006; Zhang et al., 2016). The three parameters were calculated as follows.

266
$$V_b = \begin{cases} \frac{\sqrt[3]{q \cdot g}}{0.715}, Fr < 1 \\ V_J \cdot \frac{Fr^2 + 0.4}{Fr^2}, Fr > 1 \end{cases} \quad (5)$$

267
$$Fr = \frac{V_J}{\sqrt{g \cdot d_b}} \quad (6)$$

268
$$V_e = \frac{V_b}{\cos\theta_e}, \theta_e = \arctan\left(\frac{\sqrt{2g \cdot D_H}}{V_b}\right) \quad (7)$$

269
$$\tau_j = 0.025(V/q)^{0.2} \cdot \rho_w \cdot [2g \cdot (h + d_b/2) + V_b^2] \quad (8)$$

270 2.4.3 Energy consumption of upstream area, gully head and gully bed

271 In this study, energy consumption of three landform units (upstream area, UA; gully head, GH;
 272 gully bed, GB) were calculated according to the measured runoff characteristic parameters. The
 273 bottom of GB was treated as the zero potential surface to quantify the energy consumption.
 274 Therefore, the total runoff energy (E_T , J s^{-1}), the runoff energy at the brink of headcut (E_L , J s^{-1}), the
 275 runoff energy when runoff leaves the plunge pool (E_H , J s^{-1}), and the runoff energy at the bottom of
 276 gully bed (E_B , J s^{-1}) were calculated as following.

277
$$E_T = \rho_w g q [(L_l + L_g) \tan\theta + H_h] \quad (9)$$



278
$$E_L = \rho_w g q [(L_m + L_g) \tan \theta + H_h] + \frac{1}{2} \rho_w q V_j^2 \quad (10)$$

279
$$E_H = \rho_w g q \left(L_m + L_g - V_b \sqrt{\frac{2h}{g}} \right) \tan \theta + \frac{1}{2} \rho_w q V_p^2 \quad (11)$$

280
$$E_B = \frac{1}{2} \rho_w q V_B^2 \quad (12)$$

281 where the L_l (m) and L_g (m) are the projection length of UA and GB, respectively, during gully
282 head migration; L_m (m) is the gully head retreat distance; H_h (m) is the initial gully headcut height. V_p
283 (m s⁻¹) and V_B (m s⁻¹) are the runoff velocity runoff leaving the plunge pool and GB, respectively.

284 Therefore, the total runoff energy consumption (ΔE_T , J s⁻¹), the runoff energy consumption of
285 UA (ΔE_L , J s⁻¹), the runoff energy consumption of GH (ΔE_H , J s⁻¹) and the runoff energy consumption
286 of GB (ΔE_B , J s⁻¹) could be calculated as follows.

287
$$\Delta E_T = E_T - E_B \quad (13)$$

288
$$\Delta E_L = E_T - E_L \quad (14)$$

289
$$\Delta E_H = E_L - E_H \quad (15)$$

290
$$\Delta E_B = E_H - E_B \quad (16)$$

291 2.4.4 Statistical analysis

292 The curve regression analysis method was employed to determine the quantitative relations
293 between hydraulic characteristics, jet properties, runoff energy consumption and soil erosion rate and
294 inflow discharge. The fitted equations between soil loss rate of three landform units and hydraulic
295 characteristics, jet properties, and energy consumption were also quantified by the curve regression.
296 The soil erosion volume of upstream area, gully head and gully bed were derived from the DEM of
297 different stages through the ArcGIS 10.0 software. The data analyse was executed by using SPSS
298 software (version 6.0) and figure plotting was carried out with Origin 8.5 and PowerPoint 2016
299 software.

300 3 Results

301 3.1 Spatial-temporal changes in jet properties and runoff hydraulic

302 3.1.1 Jet properties of gully head

303 Fig. 5 shows the temporal variation of three jet property parameters of gully head (GH) under
304 different inflow discharge conditions. Overall, the flow velocity at the headcut brinkpoint (V_b)



305 increased obviously in the first 30 min and then showed a gradually stable tendency with some
306 degree of fluctuation (Fig. 5a), and the fluctuation degree was enhanced as the inflow discharge
307 increased. For example, the V_b increased sharply from 0.66 to 0.88 m s⁻¹ during 100 – 124 min under
308 6.0 m³ h⁻¹ inflow discharge due to the headwall failure near headcut enhancing the runoff turbulence.
309 Regression analysis revealed the significant power relationships ($V_b=a \cdot t^b$, $R^2=0.139-0.704$, $P<0.01$)
310 between V_b and time (t) (Table 1). Furthermore, except for 3.6 m³ h⁻¹ condition, the a -value increased
311 with the inflow discharge increased, but the b -value showed a weak variation (0.08 - 0.10),
312 indicating that the flow drainage from gully head could improve initial V_b but not change its trend
313 over time. The mean V_b exhibited a significantly exponential relationship with inflow discharge (Fig.
314 5b, $P<0.05$). Contrary to the V_b , the jet velocity entry to plunge pool (V_e) and the jet shear stress (τ_j)
315 experienced a gradually decreased trend with time (Fig. 5c, 5e). Notably, the V_e and τ_j suddenly
316 decreased at 120th min and lasted nearly 40 minutes under 3.0 m³ h⁻¹ inflow discharge, which was
317 mainly attributed to the developed second headcut shortening the jet-flow height. The temporal
318 change of V_e could be described by logarithmic functions under 3.0 – 4.8 m³ h⁻¹ inflow discharge, and
319 expressed by linear functions under the other inflow discharges, whereas the decrease of the τ_j with
320 time could be presented by logarithmic functions under all inflow discharge conditions (Table 1).
321 Furthermore, both of mean V_e and τ_j could be expressed by a positive “S” function of inflow
322 discharge (Fig. 5d, 5f).

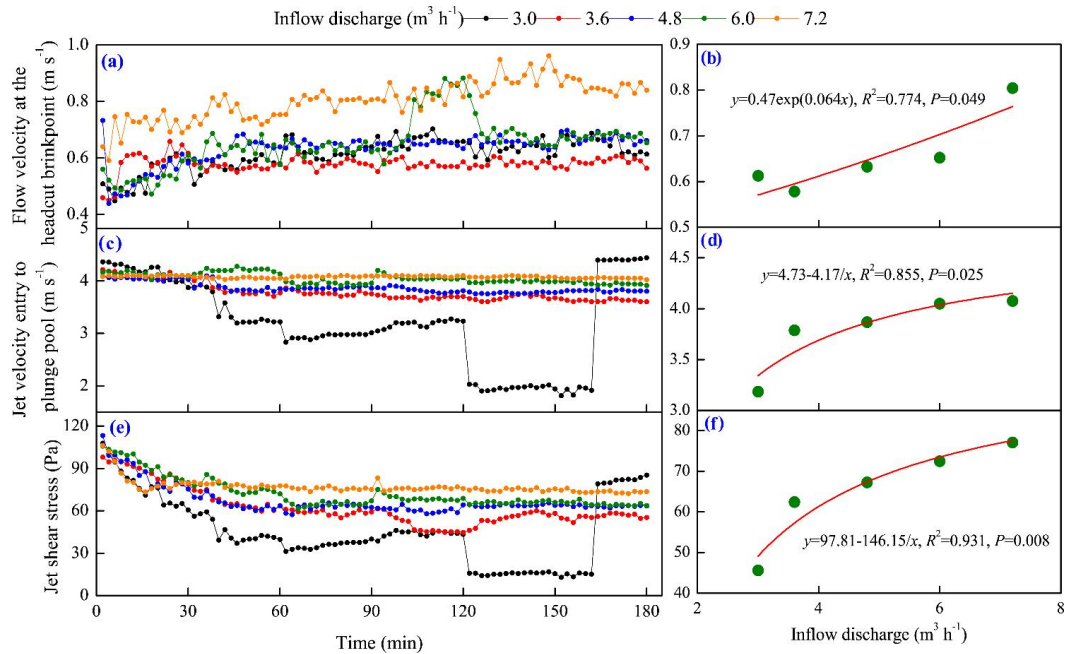


Figure 5 Temporal changes in jet properties of headcut and their relationships with inflow discharge.

Table 1 The relationships between jet properties of gully headcut and time.

Inflow discharge (m ³ h ⁻¹)	$V_b \sim t$	$V_e \sim t$	$\tau_j \sim t$
3.0	$V_b = 0.42t^{0.09}$, $R^2 = 0.691^{**}$	$V_e = 5.28 - 0.491g(t)$, $R^2 = 0.290^{**}$	$\tau_j = 110.86 - 15.441g(t)$, $R^2 = 0.344^{**}$
3.6	$V_b = 0.53t^{0.02}$, $R^2 = 0.139^{**}$	$V_e = 4.52 - 0.171g(t)$, $R^2 = 0.859^{**}$	$\tau_j = 117.93 - 13.141g(t)$, $R^2 = 0.823^{**}$
4.8	$V_b = 0.46t^{0.08}$, $R^2 = 0.544^{**}$	$V_e = 4.25 - 0.091g(t)$, $R^2 = 0.718^{**}$	$\tau_j = 109.22 - 9.931g(t)$, $R^2 = 0.770^{**}$
6.0	$V_b = 0.52t^{0.10}$, $R^2 = 0.509^{**}$	$V_e = 4.17 - 1.33 \times 10^{-3}t$, $R^2 = 0.478^{**}$	$\tau_j = 118.73 - 10.961g(t)$, $R^2 = 0.876^{**}$
7.2	$V_b = 0.57t^{0.08}$, $R^2 = 0.704^{**}$	$V_e = 4.09 - 1.38 \times 10^{-4}t$, $R^2 = 0.111^{**}$	$\tau_j = 95.68 - 4.421g(t)$, $R^2 = 0.619^{**}$

Note: V_b , V_e and τ_j are runoff velocity at the headcut brinkpoint, runoff velocity entry to plunge pool and the jet shear stress, respectively. ** refers to the significance of 0.01. The sample number is 90 for the fitted equations.

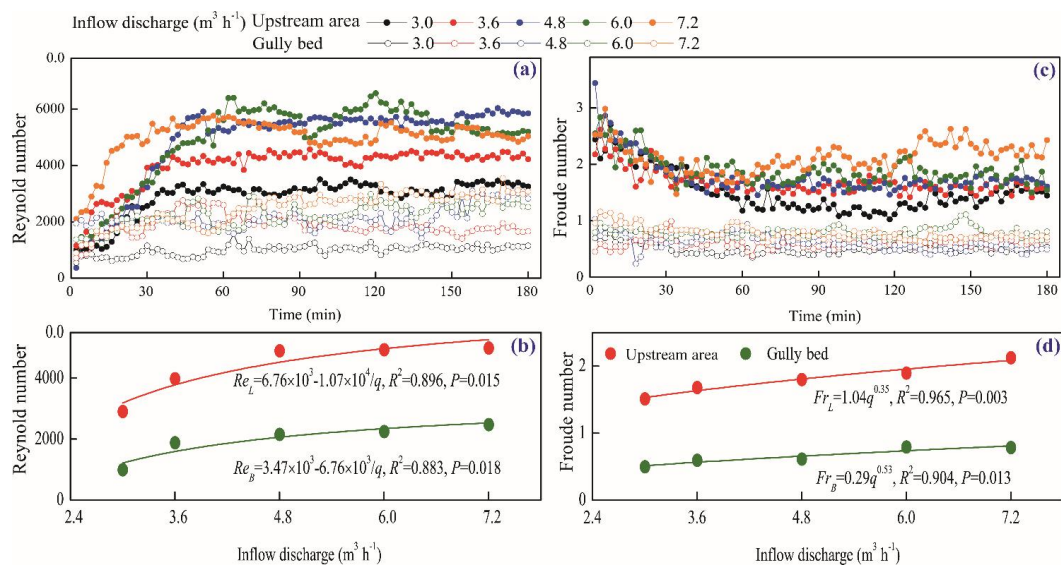
3.1.2 Runoff regime of upstream area and gully bed

The temporal changes in runoff Reynold number (Re) and Froude number (Fr) of upstream area (UA) and gully bed (GB) and their relationships with inflow discharge are provided in Fig. 6. The Re of UA and GB showed a similar trend over time, that is, the Re firstly increased in the first 40 min and then gradually stabilized (Fig. 6a). In addition, the Re of UA was larger than that of GB at any time under same inflow discharge, indicating that the runoff turbulence became weaker after the



337 runoff of UA passed the gully head. Regression analysis showed the temporal variation in Re of UA
338 could be described by logarithmic and power functions, but, for the GB, the relationship was mainly
339 dominated by power function (Table 2). On average, the Re of GB was 50.5% - 65.9% less than that
340 of UA, and the Re of UA and GB both increased with the increase of inflow discharge as a power
341 function (Fig. 6b). However, as illustrated in Fig. 6c, the Fr experienced a completely opposite trend
342 to Re . The Fr of UA decreased in the first 60 min and then gradually stabilized, but the Fr of GB
343 experienced a relatively weak-fluctuating variation over time. For the most of cases, the change in Fr
344 of UA and GB over time could be expressed by logarithmic functions (Table 2). On average, the Fr
345 of UA was 2.39-3.04 times that of GB for same inflow discharge, and the positive power function
346 could describe the relationship between Fr and inflow discharge (Fig. 6d).

347 Furthermore, the knowledge of open channel hydraulics is adopted to investigate the difference
348 in runoff regime between UA and GB. The specific definition is: the flow belongs to laminar when
349 Re is less than 500, the flow is turbulent when Re is larger than 2000, and the flow indicates
350 transitional when Re ranges from 500 to 2000; and $Fr = 1$ is the critical value for to distinguish the
351 subcritical and supercritical flow. The six flow regime zones were divided by three boundary lines
352 ($Re = 500$, $Re = 2000$, and $Fr = 1$) according to the logarithmic relationship between the flow
353 velocity and hydraulic radius (Fig. 7) (Xu et al., 2017b; Guo et al., 2020b). As shown, the runoff
354 regimes of UA and GB were located in entirely different zones. The flow of UA was in the
355 supercritical-transition flow regime in the first 26 min and then gradually transformed to
356 supercritical-turbulent flow regime under $3.0 - 6.0 \text{ m}^3 \text{ h}^{-1}$ inflow discharge, but the flow at any
357 moment was in the supercritical-turbulent regime zone under $7.2 \text{ m}^3 \text{ h}^{-1}$ inflow discharge. Moreover,
358 the higher inflow discharge would enhance the flow turbulent degree. The flow of GB belonged to
359 subcritical-laminar flow category in the initial 6 min, and then transformed to subcritical-transition
360 and subcritical-turbulent flow regime when inflow discharge was 3.0 and $3.6 \text{ m}^3 \text{ h}^{-1}$. The flow was in
361 the subcritical-turbulent flow regime in most of experimental duration when the inflow discharge is
362 $4.8 - 7.2 \text{ m}^3 \text{ h}^{-1}$. The difference in flow regime between UA and GB also indicated that the presence
363 of gully head can greatly reduce flow turbulence.



364
 365
 366
 367

Figure 6 Temporal changes in runoff regime of upstream area and gully bed and their relationships with inflow discharge.

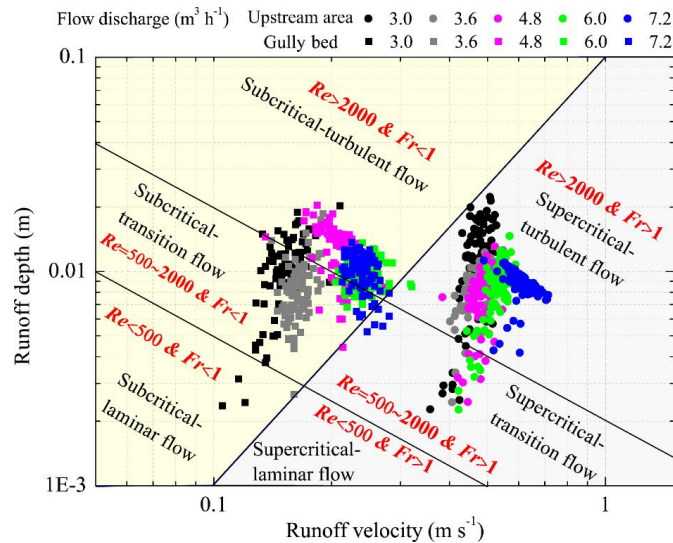


368

Table 2 Relationships between runoff hydraulic parameters and time.

Variable	Landform unit	Inflow discharge ($\text{m}^3 \text{h}^{-1}$)				
		3.0	3.6	4.8	6.0	7.2
Reynold number	UA	$Re=618.691g(t) + 286.69, R^2=0.761^{**}$	$Re=705.931g(t) + 1006, R^2=0.815^{**}$	$Re=14331g(t) - 1159, R^2=0.849^{**}$	$Re=946.64t^{0.38}, R^2=0.794^{**}$	$Re=2760t^{0.14}, R^2=0.486^{**}$
	GB	$Re=514.36t^{0.15}, R^2=0.504^{**}$	—	$Re=4.31t+1760, R^2=0.334^{**}$	$Re=1.12 \times 10^3 t^{0.16}, R^2=0.566^{**}$	$Re=744.99t^{0.28}, R^2=0.872^{**}$
Froude number	UA	$Fr=2.89-0.331g(t), R^2=0.651^{**}$	$Fr=2.46-0.191g(t), R^2=0.651^{**}$	$Fr=3.27-0.351g(t), R^2=0.656^{**}$	$Fr=2.76-0.201g(t), R^2=0.515^{**}$	—
	GB	$Fr=0.72-0.051g(t), R^2=0.326^{**}$	—	$Fr=1.0-0.091g(t), R^2=0.359^{**}$	—	$Fr=1.21-0.101g(t), R^2=0.634^{**}$
Shear stress	UA	$\tau=0.661g(t)+0.55, R^2=0.737^{**}$	$\tau=1.181g(t)+0.78, R^2=0.813^{**}$	$\tau=1.321g(t)-0.62, R^2=0.817^{**}$	$\tau=1.501g(t)-0.63, R^2=0.663^{**}$	$\tau=1.111g(t)+0.99, R^2=0.819^{**}$
	GB	$\tau=2.44t^{0.08}, R^2=0.205^{**}$	$\tau=3.88t^{0.05}, R^2=0.106^{**}$	$\tau=2.27t^{0.19}, R^2=0.664^{**}$	$\tau=3.64t^{0.12}, R^2=0.212^{**}$	$\tau=1.99t^{0.27}, R^2=0.686^{**}$
Stream power	UA	$\omega=0.341g(t)+0.16, R^2=0.761^{**}$	$\omega=0.381g(t)+0.55, R^2=0.815^{**}$	$\omega=0.781g(t)-0.63, R^2=0.849^{**}$	$\omega=0.691g(t)-0.23, R^2=0.737^{**}$	$\omega=0.271g(t)+1.56, R^2=0.436^{**}$
	GB	$\omega=0.28t^{0.15}, R^2=0.504^{**}$	$\omega=0.69t^{0.09}, R^2=0.123^{**}$	$\omega=0.50t^{0.19}, R^2=0.540^{**}$	$\omega=0.83t^{0.09}, R^2=0.338^{**}$	$\omega=0.51t^{0.23}, R^2=0.806^{**}$

369 Note: UA and GB refer to upstream area and gully bed. Re , Fr , τ and ω are Reynold number, Froude number, shear
 370 stress, stream power, respectively. ** refers to the significance of 0.01. The sample number is 90 for the fitted
 371 equations.



372

373

Figure 7 Runoff regime zones of upstream area and gully bed under different inflow discharge conditions.

374

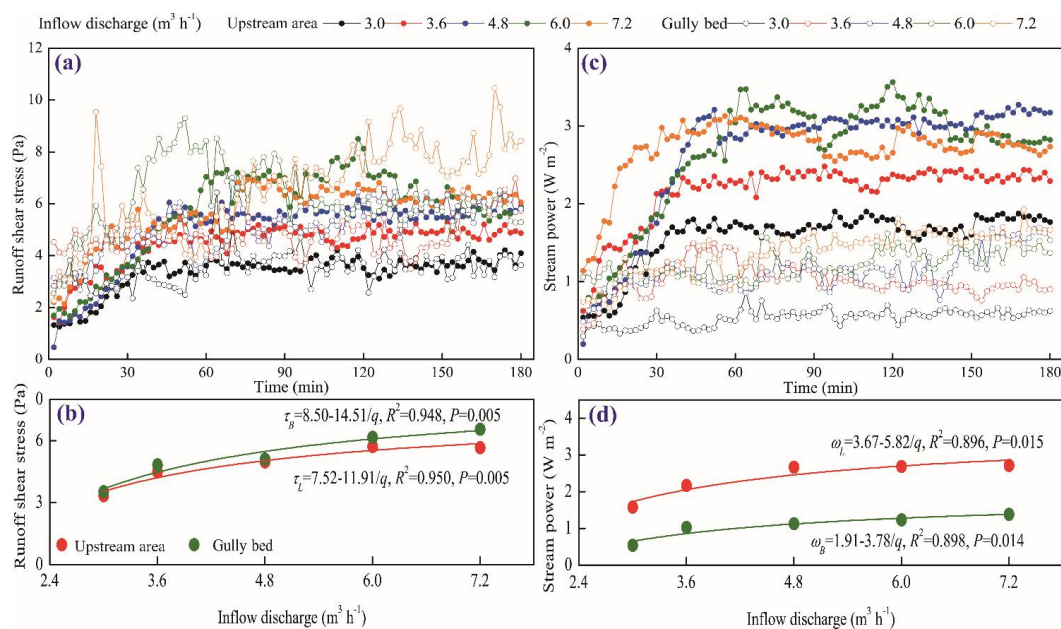
3.1.3 Runoff shear stress and stream power of upstream area and gully bed

375

Fig.8 shows the temporal changes in runoff shear stress (τ) and stream power (ω) of upstream



376 area (UA) and gully bed (GB) and their relationships with inflow discharge. Overall, the τ of UA and
 377 GB exhibited a gradually increased trend in the first 60 min, and whereafter, a relative steady state
 378 was obtained, but the larger inflow discharge perturbed the steady situation (Fig. 8a). Furthermore,
 379 the temporal change in τ of UA could be expressed by logarithmic functions, and the τ of GB
 380 showed a significant power function with experimental time (Table 2). On average, the τ of GB was
 381 2.8% - 15.7% larger than the UA. The averaged τ of UA and GB increased with inflow discharge as a
 382 power function ($\tau=a-b/q$), and the GB had a faster increased-speed (b -value) than UA (Fig. 8b),
 383 signifying that the difference in τ between UA and GB would be widened with the inflow discharge
 384 increased. Similarly, the ω of UA and GB also exhibited a trend of gradual increase and stabilization
 385 over time (Fig. 8c). Different from the temporal change in τ , the ω of GB was always less than that
 386 of UA at any time for all inflow discharge conditions. Likewise, the variation in ω of UA and GB
 387 over time exhibited a significant logarithmic and power function, respectively. On average, the ω of
 388 GB was 49.2% - 65.9% less than UA, and the positive increase in ω of UA and GB with the inflow
 389 discharge could be expressed by a power function (Fig. 8d).
 390



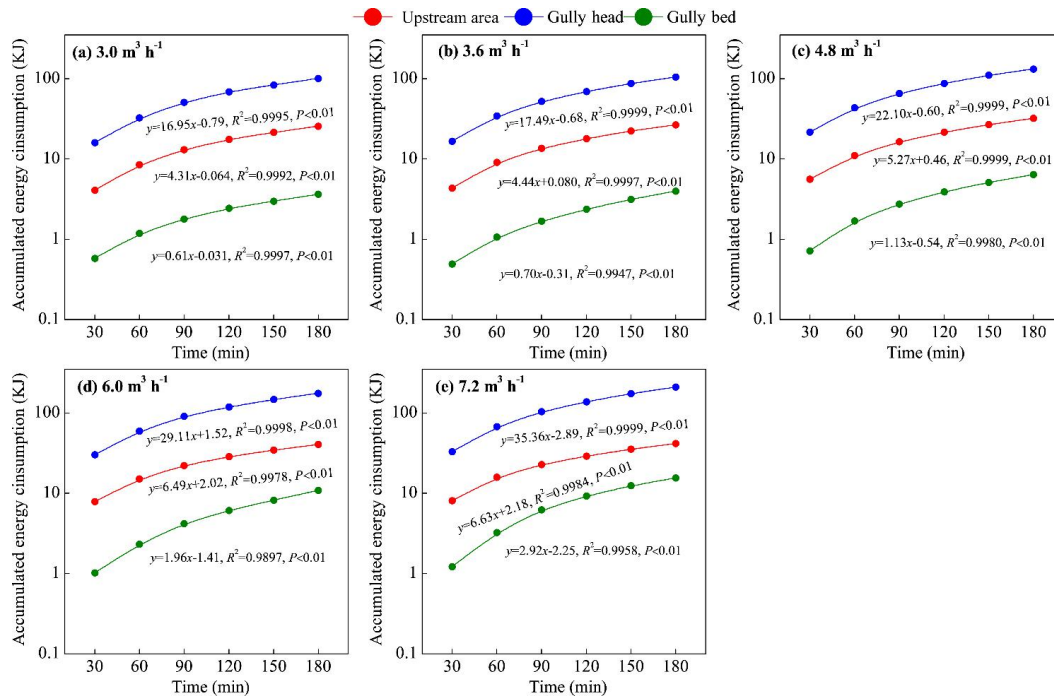
391
 392 **Figure 8** Temporal changes in runoff shear stress and stream power of upstream area and gully bed and their
 393 relationships with inflow discharge



394 3.2 Spatial-temporal change of energy consumption

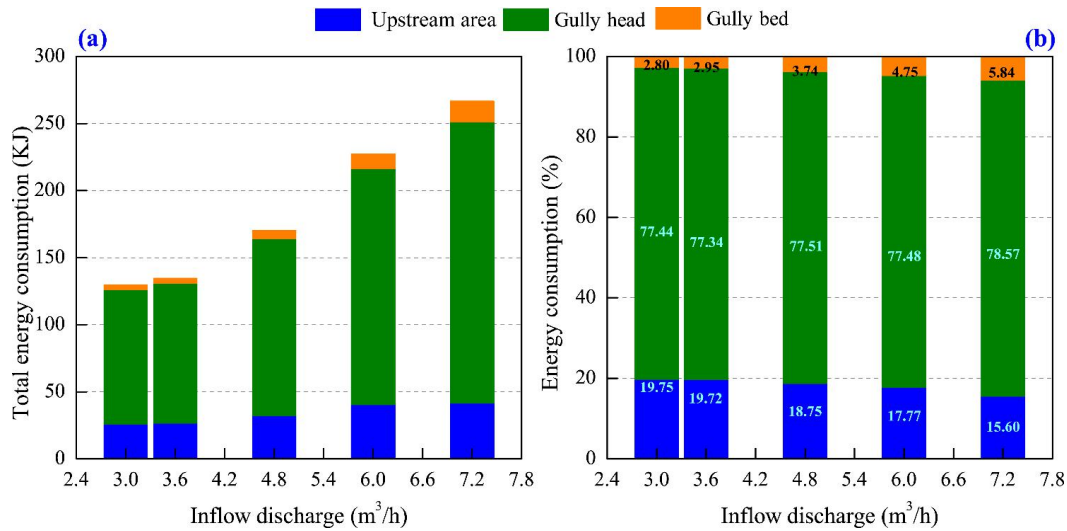
395 Fig. 9 illustrates the temporal change in accumulated energy consumption of upstream area
396 (UA), gully head (GH) and gully bed (GB). The accumulated energy consumption of the three
397 landform units continued to linearly increase with time ($R^2=0.990-0.999$, $P<0.01$), of which the
398 accumulated energy consumption in GH was always the highest at any time, followed by UA and GB
399 for the experiments of five inflow discharges. Moreover, the energy consumption rate (the
400 slope-value of fitted equation) in the three landform units is basically constant, indicating the
401 spatial-temporal change in energy consumption maintained a relatively steady state during gully
402 headcut erosion. Moreover, the energy consumption rate of GH was the highest, followed by UA and
403 GB, and the energy consumption rate in the three landform units also increased with the increase of
404 inflow discharge.

405 The variations of total energy consumption of UA, GH and GB and their proportions with
406 inflow discharge are shown in Fig. 10. As illustrated in Fig. 10a, both of the total energy
407 consumption of the “UA-GH-GB” system and the three landform units increased with the increase of
408 inflow discharge. When inflow discharge increased from 3.0 to 7.2 m³ h⁻¹, the total energy
409 consumption of the system, UA, GH and GB increased by 3.6% - 105.3%, 3.4% - 62.0%, 3.5% -
410 108.2% and 9.0% - 327.5%, respectively. Regression analysis revealed that the energy consumption
411 of system and the three landform units increased with inflow discharge as an exponential function
412 ($y=a\cdot\exp(b\cdot x)$, $a=1.14 - 55.41$, $b=0.13 - 0.36$, $R^2=0.954 - 0.992$, $P<0.05$). Furthermore, in view of the
413 proportion of energy consumption, the energy consumption of UA accounted for 15.6% - 19.8% of
414 total energy consumption, and linearly decreased with inflow discharge increased ($R^2=0.933$,
415 $P<0.05$), whereas the proportion in GB (2.8% - 5.8%) linearly increased with inflow discharge
416 increased ($R^2=0.983$, $P<0.05$). However, the proportion of energy consumption (77.3% - 78.6%) in
417 GH showed a weak change with inflow discharge (Fig. 10b), signifying that the most of runoff
418 energy (77.5% on average) was consumed in the gully head position during headcut migration.



419
 420
 421

Figure 9 Temporal changes in runoff energy consumption of upstream area, gully head and gully bed under different inflow discharge conditions



422
 423
 424

Figure 10 The variation in energy consumption of upstream area, gully head and gully bed and their proportions with inflow discharge

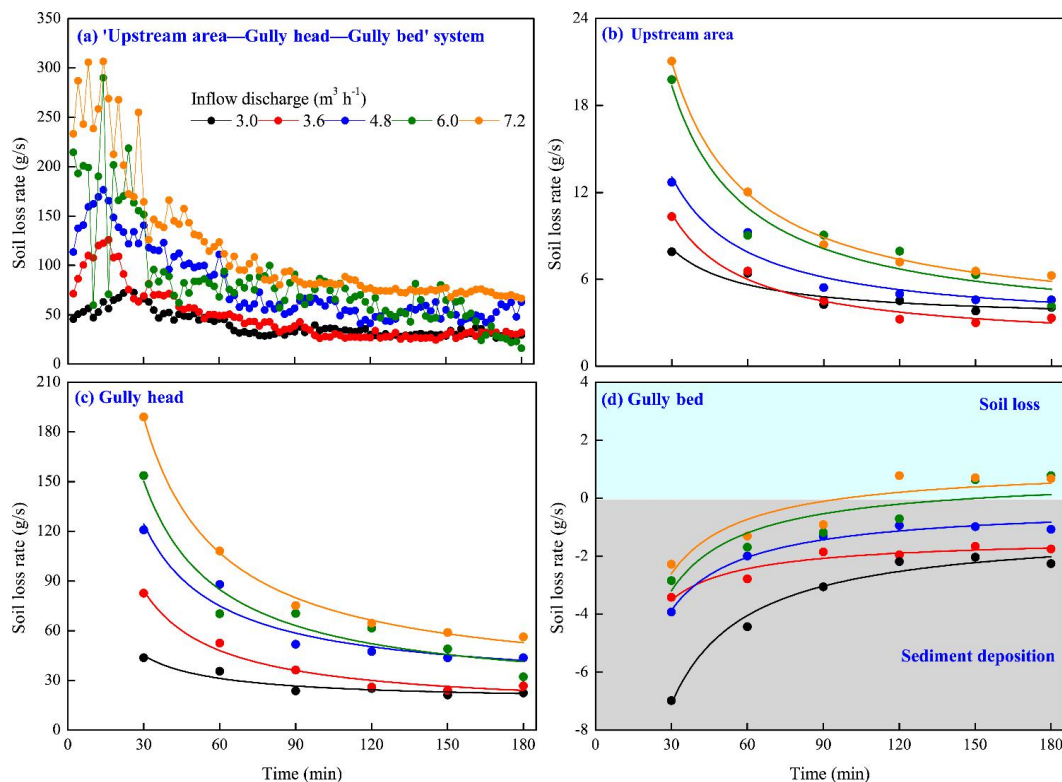


425 3.3 Spatial-temporal change of soil loss

426 3.3.1 Soil loss process

427 Fig. 11a shows that the soil loss rate of the “upstream area (UA)—gully head (GH)—gully bed
428 (GB)” system rose to a peak in first 20 min, then gradually descend and levelled off. Especially for
429 the 6.0 and 7.2 m³ h⁻¹, the soil loss rate showed a severe fluctuation trend in the first 30 min. The
430 peak soil loss rate increased from 75.4 to 306.9 g s⁻¹ with increasing inflow discharge. The soil loss
431 of UA and GH experienced a similar change process. The soil loss rate was the highest in the early
432 stage of the experiment, and gradually decreased with time, and became stable after 120 min (Fig.
433 11b, 11c). Furthermore, the temporal variation in soil loss of UA and GH could be well expressed by
434 logarithmic function ($S_L = a - b \cdot \ln(t)$, $P < 0.05$, Table 3), and the a -value (representing initial soil loss
435 rate) and b -value (reflecting the reduction rate of soil loss rate with time) increased with increasing
436 inflow discharge, indicating that larger inflow discharge can improve initial soil loss of UA and GH
437 and also expedite the decrease of soil loss rate.

438 However, the GB presented a completely different soil loss process from UA and GH (Fig. 11d).
439 The GB was always characterized by sediment deposition during the whole experiment for the 3.0 –
440 4.8 m³ h⁻¹ inflow discharges. The sediment deposition rate gradually decreased with time and
441 presented a significant “S” function over time ($S_B = a/t - b$, $R^2 = 0.918 - 0.982$, $P < 0.01$, Table 3). When the
442 inflow discharge was larger than 4.8 m³ h⁻¹, the sediment generated from UA and GH was deposited
443 firstly in the GB and then gradually transported, and the temporal change of deposited sediment on
444 GB accorded with logarithmic functions ($R^2 = 0.936$ and 0.906 , $P < 0.01$, Table 3). Furthermore, two
445 critical time points (135 min and 111 min) can be derived from the two fitted logarithmic equations,
446 which distinguished sediment deposition from sediment transport, signifying that the runoff began to
447 transport the sediment deposited on GB after 135 min and 111 min for 6.0 and 7.2 m³ h⁻¹ inflow
448 discharge.



449
 450
 451
 452
 453

Figure 11 Temporal variation in soil loss rate of the “upstream area—gully head—gully bed” system and each landform unit

Table 3 Relationships between soil loss rate of three landform units and time

Inflow discharge (m ³ h ⁻¹)	Fitted equations		
	Upstream area	Gully head	Gully bed
3.0	$S_L=15.71-2.34\ln(t)$, $R^2=0.909^{**}$	$S_H=87.12-12.99\ln(t)$, $R^2=0.908^{**}$	$S_B=-182.62/t-1.01$, $R^2=0.980^{**}$
3.6	$S_L=23.97-4.18\ln(t)$, $R^2=0.938^{**}$	$S_H=191.82-33.44\ln(t)$, $R^2=0.939^{**}$	$S_B=-64.46/t-1.36$, $R^2=0.918^{**}$
4.8	$S_L=28.76-4.85\ln(t)$, $R^2=0.930^{**}$	$S_H=273.64-46.17\ln(t)$, $R^2=0.929^{**}$	$S_B=-109.36/t-0.22$, $R^2=0.982^{**}$
6.0	$S_L=44.0-7.69\ln(t)$, $R^2=0.884^*$	$S_H=341.59-59.74\ln(t)$, $R^2=0.885^*$	$S_B=2.03\ln(t)-9.96$, $R^2=0.936^{**}$
7.2	$S_L=47.34-8.25\ln(t)$, $R^2=0.922^{**}$	$S_H=425.24-74.07\ln(t)$, $R^2=0.924^{**}$	$S_B=1.86\ln(t)-8.76$, $R^2=0.906^{**}$

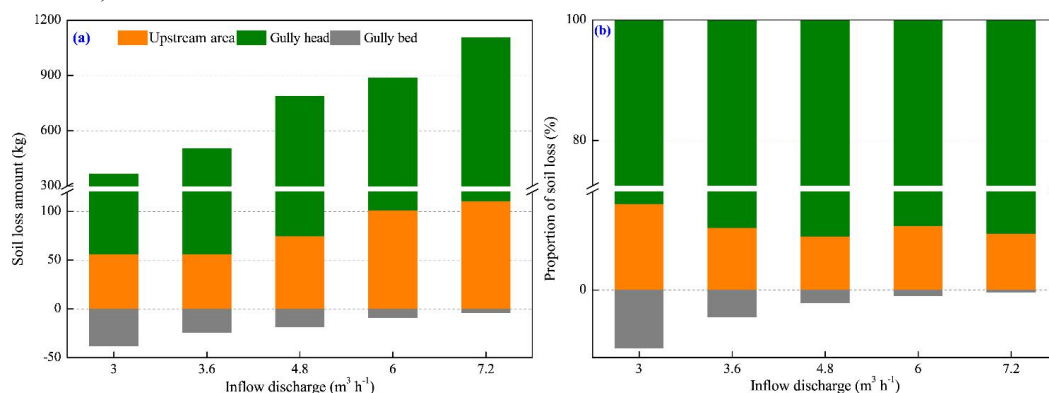
454 Note: S_L , S_H and S_B are the soil loss rate of upstream area, gully head and gully bed, respectively. The sample No. is
 455 6 for fitting equation. * and ** indicate the significant level of 0.05 and 0.01.
 456

457 3.3.2 Spatial distribution of soil loss

458 The variation in soil loss amount and proportion of the three landform units (UA, GH, GB) with
 459 inflow discharge is shown in Fig. 12. As illustrated in Fig. 12a, for the experiments of five inflow
 460 discharges, the soil loss was dominant in the UA and GH, but the GB was dominated by sediment



461 deposition due to the weaker sediment transport capacity of runoff on GB than sediment
462 deliverability of UA and GH. Furthermore, the soil loss amount of UA and GH ranged from 55.9 to
463 110.7 kg and from 310.0 to 994.8 kg, respectively, and increased linearly with increasing inflow
464 discharge ($R^2=0.966$ and 0.969 , $P<0.05$). The sediment deposition amount of GB ranged from 4.2 to
465 37.7 kg, and decreased with inflow discharge as a logarithmic function ($R^2=0.961$, $P<0.05$). In terms
466 of proportion of soil loss (Fig. 12b), the proportion of UA and GH reached the maximum (15.3%)
467 and minimum (84.7%), respectively under $3.0 \text{ m}^3 \text{ h}^{-1}$ inflow discharge, whereas, the proportion
468 exhibited a little change (UA: 9.5% - 11.4%; GH: 88.6% - 90.5%) when the inflow discharge is 7.2
469 $\text{m}^3 \text{ h}^{-1}$. Remarkably, the proportion of deposited sediment amount on GB to total soil loss amount
470 ranged from 0.4% to 10.3%, and decreased exponentially with inflow discharge ($R^2=0.992$,
471 $P<0.001$).



472
473 **Figure 12** Variation in soil loss amount and proportion of upstream area, gully head and gully bed with inflow
474 discharge
475

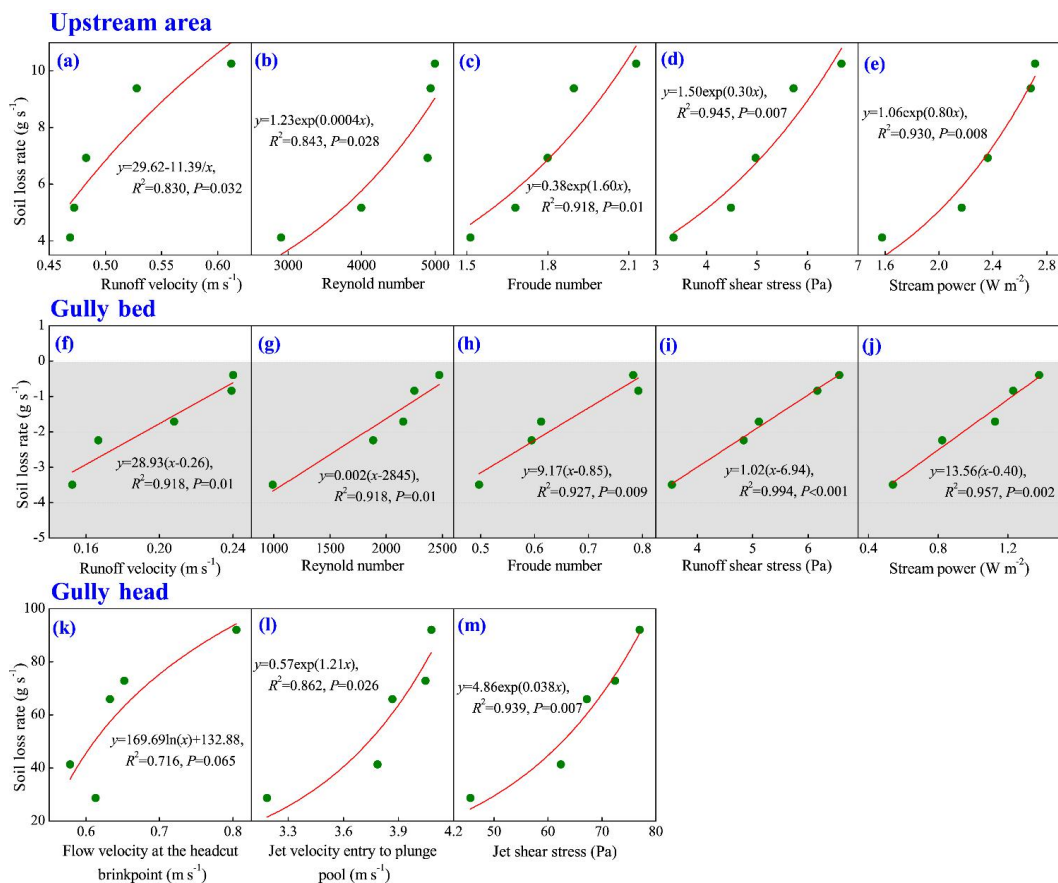
476 3.4 Spatial change in hydrodynamic mechanism of soil loss

477 3.4.1 Relationships between soil loss and hydraulic parameters

478 Fig. 13 indicates the significant difference in the relationships between soil loss rate and
479 hydraulic parameters among the three landform units (Fig. 13). For the upstream area (UA), the soil
480 loss rate could be described as a series of exponential functions of runoff velocity, Reynold number,
481 Froude number, runoff shear stress and stream power, of which the runoff shear stress and stream
482 power showed a closer correlation with soil loss (Fig. 13a - 13e, $R^2=0.830 - 0.945$). Furthermore, the



483 increased speed of soil loss rate obviously increased with the increasing hydraulic parameters (except
484 for runoff velocity), indicating that soil loss of UA showed a stronger sensitive response to increasing
485 hydraulic properties. However, the soil loss rate of gully bed (GB) linearly increased with the
486 above-mentioned five parameters (Fig. 13f – 13j, $R^2=0.918 - 0.994$), which suggested that the
487 decreased rate of sediment deposition of GB is basically constant with the increasing hydraulic
488 properties. Further analysis showed that there are critical runoff velocity, Reynold number, Froude
489 number, runoff shear stress and stream power for triggering the transformation of sediment
490 deposition to soil erosion on GB, and the critical values are 0.26 m s^{-1} , 2845, 0.85, 6.94 Pa and 0.40
491 W m^{-2} , respectively. For the gully head (GH) position, the soil loss was significantly affected by jet
492 velocity entry to plunge pool and jet shear stress (Fig. 13l and 13m, $R^2=0.862$ and 0.939), while the
493 relationship between soil loss and flow velocity at the headcut brink-point was not significant (Fig.
494 13k, $P=0.065$).

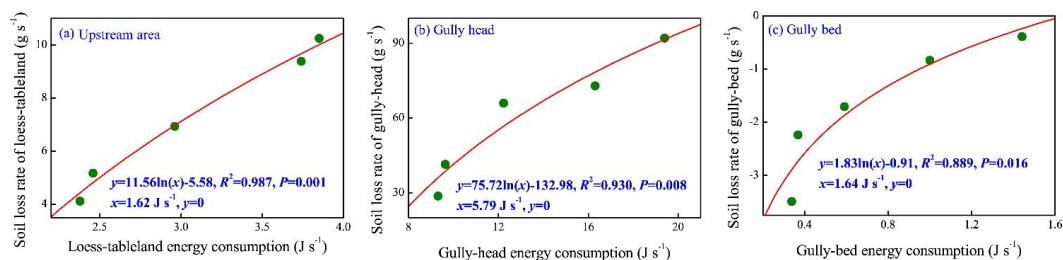


495
 496
 497

Figure 13 Relationships between soil loss rate of three landform units and hydraulic and jet properties

498 3.4.2 Response of soil loss to energy consumption

499 As illustrated in Fig. 14, the soil loss rate of three landform units was positively and
 500 significantly related to the energy consumption ($P<0.05$), and a logarithmic function was found to fit
 501 the relationship between soil loss rate and energy consumption best ($R^2=0.889 - 0.987$). Furthermore,
 502 there is critical energy consumption to initiate soil erosion of the upstream area (UA) and gully head
 503 (GH) based on the fitted logarithmic functions (Fig. 14a, b). The critical energy consumption for GH
 504 (5.79 J s^{-1}) is 2.57 times greater than that (1.62 J s^{-1}) of the UA. Similarly, for the gully bed (Fig. 14c),
 505 the minimum energy consumption (1.64 J s^{-1}) is needed to trigger the transformation of sediment
 506 deposition to soil loss.



507

508

509

Figure 14 Relationships between soil loss rate of three landform units and runoff energy consumption

510 4 Discussion

511 4.1 Spatial-temporal changes in hydraulic properties

512 This study revealed that the runoff velocity at the headcut brink-point (V_b) firstly raised and then
 513 gradually stabilized with time (Fig. 5a), which was closely corresponded to the gradually decreased
 514 runoff width on the upstream area with time (Shi et al., 2020a). However, this result was inconsistent
 515 with Zhang et al (2016, 2018) and Shi et al (2020b) who reported that the V_b decreased over time,
 516 which was mainly due to the gradually increased roughness and resistance of underlying surface over
 517 time reducing the runoff velocity (Su et al., 2015). The further analysis of power function between V_b
 518 and time ($V_b = a \cdot t^b$, Table 1) showed that the a -value increased but the b -value showed a weak
 519 variation with the inflow discharge increased, indicating that upstream flow can improve initial V_b
 520 but not affect its change trend over time. By contrast, the jet velocity entry to plunge pool (V_e) and jet
 521 shear stress (τ_j) experienced a gradually decreased process (Fig. 5c, 5e), which was mainly attributed
 522 to the shortening of jet-flow height caused by the development of second headcut and upstream flow
 523 undercutting headcut brink-point (Guo et al., 2019). This result, however, differed from the finding
 524 of Zhang et al. (2016) who stated the V_e and τ_j remained stable as the experiments progressed, which
 525 was mainly attributed to the weak change of jet-flow height induced by slow headcut retreat.

526 For the runoff hydraulic of upstream area (UA) and gully bed (GB), the Reynold number Re of
 527 UA and GB initially increased and gradually stabilized, but the Froude number Fr showed an
 528 opposite trend. This phenomenon was agreed with previous studies (e.g. Su et al., 2015; Zhang et al.,
 529 2016; Shi et al., 2020a). Besides, for the same upstream inflow discharge, the Re and Fr of UA were
 530 larger than that of GB by 50.5%-65.9% and 1.39-2.04 times, respectively, indicating that the runoff



531 turbulence became weaker after the runoff of UA passed the gully head and plunge pool. More
532 evidently, the runoff on UA was in the supercritical-transition and supercritical-turbulent flow regime
533 ($Re > 500$, $Fr > 1$), whereas the runoff on GB belonged to subcritical-transition and
534 subcritical-turbulent flow regime ($Re > 500$, $Fr < 1$). The above result was supported by Shi et al.
535 (2020a) who stated that the Re of gully bed decreased by 1.5%-30% as the flow fell from the
536 upstream area, but Su et al. (2015) suggested that the steady state Re of gully bed was higher than
537 that of upstream area. In the study of Su et al. (2015), the larger gully bed slope gradient than
538 upstream area would accelerate the runoff velocity and thus enhance flow turbulence (Bennett, 1999;
539 Pan et al., 2016). Our study found that temporal variation in the shear stress (τ) and stream power (ω)
540 of UA was similar with GB, and, compared to UA, the τ and ω of GB increased and decreased by
541 2.8% - 15.7% and 49.2% - 65.9%, respectively. This was different from some previous experimental
542 studies on gully and bank gully. For example, the result from the study of Shi et al. (2020a) indicated
543 that the τ of gully bed decreased by 65.9% - 67.1%, compared to catchment area, and a similar result
544 was also found during bank gully headcut erosion (Su et al., 2015). Previous studies also have
545 proven that the change in hydraulic properties from upstream area to gully bed is affected by various
546 factors including plunge pool size, slope gradient, initial step height, and soil texture (Bennett and
547 Casalí, 2001; Wells et al., 2009a, 2009b).

548 **4.2 Spatial-temporal change in runoff energy consumption and soil erosion**

549 Our study revealed that the accumulated runoff energy consumption of the upstream area (UA),
550 gully headcut (GH) and gully bed (GB) linearly increased over time (Fig. 9), indicating the
551 spatial-temporal change in energy consumption maintained a relatively steady state during gully
552 headcut erosion. However, the flow energy consumption of bank gully in three landform units
553 logarithmically increased over time (Su et al., 2015). This difference further manifested that the
554 runoff energy consumption of different landform units depends on gully type to some extent as well
555 as soil texture, slope and headwall height (Wells et al., 2009a). Besides, under this flow discharge
556 conditions, the proportion of energy consumption in UA, GH and GB was 15.6%-19.8%,
557 77.3%-78.6% and 2.8%-5.8%, respectively (Fig. 10), which was also indirectly supported by the
558 study of Su et al. (2015) who suggested that the runoff energy consumption per unit soil loss from



559 upstream area, headcut and gully bed is 17.4%, 70.5% and 12.0%, respectively. This further signified
560 that the gully head consumed the most of runoff energy (77.5% on average) during headcut
561 migration. The flow energy must be consumed to surmount the soil resistance as headcut migrates,
562 and the consumed energy was mainly focused on headwall and plunge pool development (Alonso et
563 al., 2002).

564 In terms of soil loss, our study indicated that the soil loss rate of the “UA-GH-GB” system
565 initially increased to the peak value and then gradually declined and stabilized (Fig. 11), which was
566 consistent with the results of many studies on rill and gully headcut erosion under different
567 conditions (slope, initial step height, flow discharge, soil type, soil stratification) (Bennett, 1999;
568 Bennett and Casalí, 2001; Gordon et al., 2007; Wells et al., 2009a; Shi et al., 2020a). Both the scour
569 depth and sediment production increased in the initial period of underlying surface adjustment, while
570 once the plunge pool development was maintained, and sediment yield decreased and gradually
571 stabilized (Bennett et al., 2000). In addition, the significant difference in soil loss process was found
572 among the three landform units. The soil loss of UA and GH decreased logarithmically over time,
573 which was similar with several studies (e.g. Su et al., 2015; Shi et al., 2020b). Nevertheless, the GB
574 was always characterized by sediment deposition for the inflow discharge of $< 4.8 \text{ m}^3 \text{ h}^{-1}$, whereas
575 the sediment was deposited firstly and then gradually transported as the inflow discharge increased to
576 6.0 and $7.2 \text{ m}^3 \text{ h}^{-1}$. Similar results were also found in some previous studies on rill heacut erosion
577 (Bennett, 1999; Bennett and Casalí, 2001; Gordon et al., 2007; Wells et al., 2009a). However, Su et
578 al. (2014, 2015) revealed a larger soil loss volume or soil loss rate in gully bed than upstream area
579 and headwall during bank gully headcut erosion. This difference between our study and Su et al.
580 (2014, 2015) is primarily caused by the difference in slope gradient. The gully bed slope (20°) of
581 bank gully was larger than that (3°) of our study, indicating the runoff on gully bed of bank gully
582 had stronger sediment transport capacity (Zhang et al., 2009; Ali et a., 2013; Wu et al., 2016, 2018).
583 In view of the proportion of soil loss, the proportion of UA and GH was 9.5% - 11.4% and 88.6% -
584 90.5%, respectively, of which the proportion of deposited sediment on GB to the sediment yield from
585 UA and GH can reach up to 0.4% - 10.3%. This result fully demonstrated that the gully head is the
586 main source of sediment production during gully headcut erosion (Oostwoud-Wijdenes & Bryan,



587 1994; Zhao, 1994; Su et al., 2014), and also manifested the necessary and importance of gully
588 headcut erosion controlling in gully-dominated region.

589 **4.3 Hydrodynamic characteristics of headcut erosion**

590 The significant different relationships between soil loss and jet or hydraulic characteristics was
591 found among UA, GH, and GB. The soil loss rate of UA exponentially increased with five hydraulic
592 parameters (runoff velocity, Reynold number, Froude number, runoff shear stress and stream power),
593 indicating that soil loss of UA showed a stronger sensitive response to increasing hydraulic
594 properties. This could attribute to the frequent bank collapse on UA accelerating soil loss (Wells et
595 al., 2013; Qin et al., 2018). However, the sediment deposition rate of GB linearly decreased with the
596 five hydraulic parameters, signifying that sediment deposition on GB decreased at a stable state with
597 the increase of hydraulic parameters. Therefore, the sediment deposition rate would reach zero when
598 the five hydraulic parameters increased to the critical values, implying that the transformation of
599 sediment deposition to sediment transport on GB would be triggered. Furthermore, the shear stress is
600 the optimal parameter describing soil loss process of UA and GB, which differed from some studies
601 on hillslope erosion hydrodynamic characteristics (Zhang et al., 2009; Shen et al., 2019; Ma et al.,
602 2020). Most of studies have verified that stream power is the superior hydrodynamic parameter
603 describing soil detachment process. This comparison also fully illustrated the great difference in
604 hydrodynamic characteristic between hillslope erosion and headcut erosion. In this study, the soil
605 loss of gully head (including plunge pool erosion) was significantly affected by jet properties. It's
606 confirmed that the plunge pool erosion by jet flow becomes a crucial process controlling gully head
607 migration and sediment production (Oostwoud-Wijdenes et al., 2000). Consequently, the plunge pool
608 erosion theory is usually employed to build several headcut retreat models (Alonso et al., 2002;
609 Campo-Bescós et al., 2013). Although the weak correlation between soil loss of gully head and flow
610 velocity at headcut breakpoint, the larger flow velocity resulted from increasing inflow discharge
611 would improve the shear stress of jet flow impinging gully bed, and thus the gully headcut suffered
612 stronger incisional erosion of the plunge pool. However, in fact, the soil loss of gully head was also
613 affected by on-wall flow erosion (Chen et al., 2013), and thus more studies should be conducted to
614 clear the effect of on-wall flow properties on headcut erosion.



615 From the energy consumption perspective, the soil loss rate of the three landform units
616 significantly and logarithmically increased with the energy consumption, and the similar change
617 trend was also found in the study of Su et al. (2015). This finding suggests that energy consumption
618 could be considered as the available parameter to estimate the soil loss of gully headcut erosion (Shi
619 et al., 2020b). Furthermore, we found the critical energy consumption initiating soil erosion of UA,
620 GH, and GB are 1.62 J s^{-1} , 5.79 J s^{-1} and 1.64 J s^{-1} , respectively, indicating the soil loss of gully head
621 (including plunge pool) needs more flow energy consumption (Zhang et al., 2018; Shi et al., 2020a,
622 2020b). This phenomenon can be attributed to the fact that the more runoff energy was consumed at
623 the gully headwall and plunge pool erosion than UA and GB and thus resulted in more severe soil
624 loss during headcut erosion.

625 **Summary**

626 This study investigated the temporal-spatial changes in flow hydraulic, energy consumption and
627 soil loss during headcut erosion based on a series of scouring experiments of gully headcut erosion.
628 The jet properties of gully head (GH) were significantly affected by upstream flow discharge. The
629 upstream area (UA) and gully bed (GB) had similar temporal changes in Reynold number, Froude
630 number, shear stress and stream power. The flow was supercritical on UA, but subcritical on GB, and
631 the turbulent degree was enhanced by the increasing inflow discharge. The flow Reynold number,
632 shear stress and stream power decreased by 56.0%, 63.8% and 55.9%, respectively, but Froude
633 number increased by 7.9% when flow passed the gully headcut and plunge pool. The accumulated
634 energy consumption at UA, GH and GB linearly increased with time, of which the GH consumed
635 77.5% of the total runoff energy. The soil loss of UA and GH decreased logarithmically over time,
636 whereas the GB was mainly characterized by sediment deposition. The GH can contribute 88.5% of
637 total soil loss, of which 3.8% sediment production was deposited on GB. The soil loss of UA and GH
638 and the sediment deposition of GB were significantly affected by hydraulic and jet properties. Our
639 study revealed that the critical energy consumption to initiate soil erosion of UA, GH and GB are
640 1.62 J s^{-1} , 5.79 J s^{-1} and 1.64 J s^{-1} , respectively. The runoff energy consumption could be considered
641 as a non-negligible parameter to predict soil loss of gully headcut erosion.



642 **Data availability**

643 At present, the data are not publicly accessible because of a situation that we don't have permission
644 to share data according to the requirement of the funded program and our institute.

645 **Author contribution**

646 Mingming Guo and Wenlong Wang designed the experiments. Mingming Guo, Zhuoxin Chen,
647 Tianchao Wang, Qianhua Shi, Man Zhao and Lanqian Feng carried out the experiments. Zhuoxin
648 Chen produced and processed the digital elevation model of erosion landform. Mingming Guo and
649 Wennlong Wang written and prepared the manuscript with contributions from all co-authors.

650 **Competing interests:**

651 The authors declare that they have no conflict of interest.

652 **Acknowledgments**

653 This work was supported by the National Natural Science Foundation of China (41571275) and
654 the National Key Research and Development Program of China (2016YFC0501604).
655 Acknowledgement for the data support from "Loess Plateau Data Center, National Earth System
656 Science Data Sharing Infrastructure, National Science & Technology Infrastructure of China.
657 (<http://loess.geodata.cn>)".

658 **References**

- 659 Addisie, M.B., Ayele, G.K., Gessess, A.A., Tilahun, S.A., Zegeye, A.D., Moges, M.M., ... Steenhuis, T.S.:
660 Gully head retreat in the sub-humid Ethiopian Highlands: The Ene-Chilala catchment, *Land Degradation &*
661 *Development*, 28, 1579–1588, <https://doi.org/10.1002/ldr.2688>, 2017.
- 662 Ali, M., Seeger, M., Sterk, G., Moore, D.: A unit stream power based sediment transport function for overland
663 flow. *Catena*, 101, 197-204. <https://doi.org/10.1016/j.catena.2012.09.006>
- 664 Alonso, C.V., Bennett, S.J., Stein, O.R., 2002. Predicting head cut erosion and migration in concentrated flows
665 typical of upland areas, *Water Resources Research*, 38, 39-1–39-15, <http://dx.doi.org/10.1029/2001WR001173>,
666 2013.
- 667 Beer, C.E., Johnson, H.P.: Factors in gully growth in the deep loess area of western Iowa. *Transactions of*
668 *ASAE*, 6, 237–240, <https://doi.org/10.13031/2013.40877>, 1963.
- 669 Bennett, S.J., Casali, J.: Effect of initial step height on headcut development in upland concentrated flows.
670 *Water Resources Research*, 37, 1475–1484, <https://doi.org/10.1029/2000WR900373>, 2001.
- 671 Bennett, S.J.: Effect of slope on the growth and migration of headcuts in rills, *Geomorphology*, 30, 273–290,
672 [https://doi.org/10.1016/S0169-555X\(99\)00035-5](https://doi.org/10.1016/S0169-555X(99)00035-5), 1999.



- 673 Bennett, S.J., Alonso, C.V.: Turbulent flow and bed pressure within headcut scour holes due to plane
674 reattached jets, *Journal of Hydraulic Research*, 44, 510–521, <https://doi.org/10.1080/00221686.2006.9521702>,
675 2006.
- 676 Bennett, S.J., Alonso, C.V., Prasad, S.N., Romkens, M.J.: Experiments on headcut growth and migration in
677 concentrated flows typical of upland areas, *Water Resources Research*, 36, 1911–1922,
678 <https://doi.org/10.1029/2000WR900067>, 2000.
- 679 Campo-Bescós, M.A., Flores-Cervantes, J.H., Bras, R.L., Casalí, J., Giráldez, J.V.: Evaluation of a gully
680 headcut retreat model using multitemporal aerial photographs and digital elevation models, *Journal of*
681 *Geophysical Research: Earth Surface*, 118, 2159–2173, <https://doi.org/10.1002/jgrf.20147>, 2013.
- 682 Chaplot, V., Giboire, G., Marchand, P., Valentin, C.: Dynamic modelling for linear erosion initiation and
683 development under climate and land-use changes in northern Laos, *Catena*, 63, 318–328,
684 <https://doi.org/10.1016/j.catena.2005.06.008>, 2005.
- 685 Che, X.L.: Study of distribution characteristic and evolution of headward erosion on Dongzhi tableland of the
686 loess gully region, Yangling: Northwest A&F University, pp. 66–67, (In Chinese), 2012.
- 687 Chen, A., Zhang, D., Peng, H., Fan, J., Xiong, D., Liu, G.: Experimental study on the development of collapse
688 of overhanging layers of gully in Yuanmou Valley, China, *Catena*, 109, 177–185,
689 <https://doi.org/10.1016/j.catena.2013.04.002>, 2013.
- 690 De Baets, S., Poesen, J., Knäpen, A., Galindo, P.: Impact of root architecture on the erosion-reducing potential
691 of roots during concentrated flow, *Earth Surface Processes and Landforms*, 32, 1323–1345,
692 <https://doi.org/10.1002/esp.1470>, 2007.
- 693 de Vente, J., Poesen, J.: Predicting soil erosion and sediment yield at the basin scale: Scale issues and
694 semi-quantitative models, *Earth-Science Reviews*, 71, 95–125, <https://doi.org/10.1016/j.earscirev.2005.02.002>,
695 2005.
- 696 DeLong, S.B., Johnson, J., Whipple, K.: Arroyo channel head evolution in a flash-flood-dominated
697 discontinuous ephemeral stream system, *Geological Society of America Bulletin*, 126, 1683–1701,
698 <https://doi.org/10.1130/B31064.1>, 2014.
- 699 Descroix, L., González Barrios, J.L., Viramontes, D., Poulenard, J., Anaya, E., Esteves, M., Estrada, J.: Gully
700 and sheet erosion on subtropical mountain slopes: their respective roles and the scale effect, *Catena*, 72,
701 325–339, <https://doi.org/10.1016/j.catena.2007.07.003>, 2008.
- 702 Dotterweich, M., Rodzik, J., Zglobicki, W., Schmitt, A., Schmidtchen, G., Bork, H.R.: High resolution gully
703 erosion and sedimentation processes, and land use changes since the Bronze Age and future trajectories in the
704 Kazimierz Dolny area (Nałęczów Plateau, SE-Poland), *Catena*, 95, 50–62,
705 <https://doi.org/10.1016/j.catena.2012.03.001>, 2012.
- 706 Flores-Cervantes, J., Istanbuloglu, E., Bras, R.: Development of gullies on the landscape: A model of
707 headcut retreat resulting from plunge pool erosion, *Journal of Geophysical Research*, 111, 1–14,
708 <https://doi.org/10.1029/2004JF000226>, 2006.
- 709 Frankl, A., Stal, C., Abraha, A., Nyssen, J., Rieke-Zapp, D., DeWulf, A., Poesen, J.: Detailed recording of
710 gully morphology in 3D through image-based modelling, *Catena*, 127, 92–101,
711 <https://doi.org/10.1016/j.catena.2014.12.016>, 2015.
- 712 Fu, B.J., Liu, Y., Lv, Y.H., He, C.S., Zeng, Y., Wu, B.F.: Assessing the soil erosion control service of
713 ecosystems change in the Loess Plateau of China, *Ecological Complexity*, 8, 284–293,
714 <https://doi.org/10.1016/j.ecocom.2011.07.003>, 2011.



- 715 Gordon, L.M., Bennett, S.J., Wells, R.R., Alonso, C.V.: Effect of soil stratification on the development and
716 migration of headcuts in upland concentrated flows, *Water Resources Research*, 43, W07412,
717 <https://doi.org/10.1029/2006WR005659>, 2007.
- 718 Guo, M., Wang, W., Shi, Q., Chen, T., Kang, H., Li, J.: An experimental study on the effects of grass root
719 density on gully headcut erosion in the gully region of China's Loess Plateau, *Land Degradation &*
720 *Development*, 30, 2107–2125, <https://doi.org/10.1002/ldr.3404>, 2019.
- 721 Guo, M., Wang, W., Wang, T., Wang, W., Kang, H.: Impacts of different vegetation restoration options on
722 gully head soil resistance and soil erosion in loess tablelands, *Earth Surface Processes and Landforms*, 45(4),
723 1038–1050, <https://doi.org/10.1002/esp.4798>, 2020.
- 724 Guo, M.M., Wang, W.L., Kang, H.L., Yang, B.: Changes in soil properties and erodibility of gully heads
725 induced by vegetation restoration on the Loess Plateau, China, *Journal of Arid Land*, 10(5), 712–725,
726 <https://doi.org/10.1007/s40333-018-0121-z>, 2018.
- 727 Guo, M.M., Wang, W.L., Li, J.M., Bai, Y., Kang, H.L., Yang, B.: Runoff characteristics and soil erosion
728 dynamic processes on four typical engineered landforms of coalfields: An in-situ simulated rainfall
729 experimental study, *Geomorphology* 349, 106896, <https://doi.org/10.1016/j.geomorph.2019.106896>, 2020.
- 730 Hager, W.H.: Hydraulics of plane free overfall, *Journal of Hydraulic Engineering*, 109, 1683–1697,
731 [https://doi.org/10.1061/\(ASCE\)0733-9429\(1983\)109:12\(1683\)](https://doi.org/10.1061/(ASCE)0733-9429(1983)109:12(1683)), 1983.
- 732 Hanson, G.J., Robinson, K.M., Cook, K.R.: Prediction of headcut migration using a deterministic approach,
733 *Transactions of the ASAE*, 44(4), 525–531, <https://doi.org/10.13031/2013.6112>, 2001.
- 734 Hosseinalizadeh, M., Kariminejad, N., Chen, W., Pourghasemi, H.R., Alinejad, M., Behbahani, A.M.,
735 Tiefenbacher, J.P.: Gully headcut susceptibility modeling using functional trees, naïve Bayes tree, and random
736 forest models, *Geoderma*, 342, 1–11, <https://doi.org/10.1016/j.geoderma.2019.01.050>, 2019.
- 737 Ionita, I.: Gully development in the Moldavian Plateau of Romania, *Catena*, 68, 133–140,
738 <https://doi.org/10.1016/j.catena.2006.04.008>, 2006.
- 739 Ionita, I., Niacsu, L., Petrovici, G., Blebea-Apostu, A.M.: Gully development in eastern Romania: a case study
740 from Falcui Hills, *Natural Hazards*, 79, 113–138, <https://doi.org/10.1007/s11069-015-1732-8>, 2015.
- 741 Jiao, J.Y., Wang, W.Z., Hao, X.P.: Precipitation and erosion characteristics of rainstorm in different pattern on
742 Loess Plateau, *Journal of Arid Land Resources and Environment*, 13(1), 34–42, (In Chinese), 1999.
- 743 Kirkby, M.J., Bull, L.J., Poesen, J., Nachtergaele, J., Vandekerckhove, L.: Observed and modelled
744 distributions of channel and gully heads—with examples from SE Spain and Belgium, *Catena*, 50, 415–434,
745 [https://doi.org/10.1016/S0341-8162\(02\)00128-5](https://doi.org/10.1016/S0341-8162(02)00128-5), 2003.
- 746 Li, Binbing., Huang, Lei., Feng, Lin., Li, Peng., Yao, Jingwei., Liu, Fangming., Li, Junli., Tang, Hui.: Gully
747 sidewall expansion process on loess hill slope erosion, *Journal of Basic Science and Engineering*, 24(6),
748 1147–1158. (In Chinese), 2016.
- 749 Li, H., Cruse, R.M., Liu, X.B., Zhang, X.Y.: Effects of topography and land use change on gully development
750 in typical Mollisol region of Northeast China, *Chinese Geographical Science*, 26, 779–788,
751 <https://doi.org/10.1007/s11769-016-0837-7>, 2016.
- 752 Li, M., Song, X.Y., Shen, B., Li, H.Y., Meng, C.X.: Influence of vegetation change on producing runoff and
753 sediment in gully region of Loess Plateau, *Journal of Northwest Sci-Tech University of AgriculAure and*
754 *Forestry (Natural Science Edition)*, 34, 117–120, (In Chinese), 2006.



- 755 Li, Z., Zhang, Y., Zhu, Q., He, Y., Yao, W.: Assessment of bank gully development and vegetation coverage on
756 the Chinese Loess Plateau, *Geomorphology*, 228, 462–469, <https://doi.org/10.1016/j.geomorph.2014.10.005>,
757 2015.
- 758 Li, Z., Zheng, F.L., Liu, W.Z., Flanagan, D.C.: Spatial distribution and temporal trends of extreme temperature
759 and precipitation events on the Loess Plateau of China during 1961–2007, *Quaternary International*, 226(1-2),
760 92–100, <https://doi.org/10.1016/j.quaint.2010.03.003>, 2010.
- 761 Ma, Q., Zhang, K., Cao, Z., Wei, M., & Yang, Z.: Soil detachment by overland flow on steep cropland in the
762 subtropical region of China, *Hydrological Processes*, 34(8), 1810–1820, <https://doi.org/10.1002/hyp.13694>,
763 2020
- 764 Martínez-Casasnovas, J.A., Concepción Ramos, M., García-Hernández, David.: Effects of land - use changes
765 in vegetation cover and sidewall erosion in a gully head of the Penedès region (northeast Spain), *Earth Surface*
766 *Processes & Landforms*, 34, 1927–1937, <https://doi.org/10.1002/esp.1870>, 2009.
- 767 Nazari Samani, A., Ahmadi, H., Mohammadi, A., Ghoddousi, J., Salajegheh, A., Boggs, G., Pishyar, R.:
768 Factors Controlling Gully Advancement and Models Evaluation (Hableh Rood Basin, Iran), *Water Resources*
769 *Management*, 24, 1532–1549, <https://doi.org/10.1007/s11269-009-9512-4>, 2010.
- 770 Oostwoud-Wijdenes, D., Bryan, R.B.: The significance of gully headcuts as a source of sediment on low-angle
771 slopes at Baringo, Kenya, and initial control measures, *Advances in Geocology*, 27, 205–231, 1994.
- 772 Oostwoud-Wijdenes, D., Poesen, J., Vandekerckhove, L., Ghesquiere, M.: Spatial distribution of gully head
773 activity and sediment supply along an ephemeral channel in a Mediterranean environment, *Catena*, 39,
774 147–167, [http://202.194.143.28:80/rwt/SD/https/MSYXTLUQPJUB/10.1016/S0341-8162\(99\)00092-2](http://202.194.143.28:80/rwt/SD/https/MSYXTLUQPJUB/10.1016/S0341-8162(99)00092-2), 2000.
- 775 Pan, C., Ma, L., Wainwright, J., Shangguan, Z.: Overland flow resistances on varying slope gradients and
776 partitioning on grassed slopes under simulated rainfall, *Water Resources Research*, 52, 2490–2512,
777 <https://doi.org/10.1002/2015WR018035>, 2016.
- 778 Poesen, J., Nachtergaele, J., Verstraeten, G., Valentin, C.: Gully erosion and environmental change:
779 Importance and research needs, *Catena*, 50, 91–133, [https://doi.org/10.1016/S0341-8162\(02\)00143-1](https://doi.org/10.1016/S0341-8162(02)00143-1), 2003.
- 780 Qin, Chao., Zheng, Fenli., Wells Robert, R., Xu, Ximeng, Wang, Bin., Zhong, Keyuan.: A laboratory study of
781 channel sidewall expansion in upland concentrated flows, *Soil and Tillage Research*, 178, 22–31,
782 <https://doi.org/10.1016/j.still.2017.12.008>, 2018.
- 783 Reuter, H.I., Nelson, A., Jarvis, A.: An evaluation of void filling interpolation methods for SRTM data,
784 *International Journal of Geographic Information Science*, 21(9), 983–1008, 2007.
- 785 Rieke-Zapp, D.H., Nichols, M.H.: Headcut retreat in a semiarid watershed in the southwestern United States
786 since 1935, *Catena*, 87, 1–10, <https://doi.org/10.1016/j.catena.2011.04.002>, 2011.
- 787 Rodzik, J., Furtak, T., Zglobicki, W.: The impact of snowmelt and heavy rainfall runoff on erosion rates in a
788 gully system, Lublin Upland, Poland, *Earth Surface Processes & Landforms*, 34, 1938–1950,
789 <https://doi.org/10.1002/esp.1882>, 2009.
- 790 Rouse, H.: *Engineering hydraulics*. Hoboken, NJ: Wiley, 1950.
- 791 Sanchis, M.P., Torri, D., Borselli, L., Poesen, J.: Climate effects on soil erodibility, *Earth Surface Processes &*
792 *Landforms*, 33, 1082–1097, <https://doi.org/10.1002/esp.1604>, 2008.
- 793 Shen, N., Wang, Z., Zhang, Q., Chen, H., Wu, B.: Modelling soil detachment capacity by rill flow with
794 hydraulic variables on a simulated steep loessial hillslope, *Hydrology Research*, 50(1), 85–98,
795 <https://doi.org/10.2166/nh.2018.037>, 2018.



- 796 Shi, Q.H., Wang, W.L., Guo, M.M., Chen, Z.X., Feng, L.Q., Zhao, M., Xiao, H.: The impact of flow discharge
797 on the hydraulic characteristics of headcut erosion processes in the gully region of the Loess Plateau,
798 Hydrological processes, 34, 718-729, <https://doi.org/10.1002/hyp.13620>, 2020.
- 799 Shi, Q., Wang, W., Zhu, B., Guo, M.: Experimental study of hydraulic characteristics on headcut erosion and
800 erosional response in the tableland and gully regions of China, Soil Science Society of America Journal, 84,
801 700–716, <https://doi.org/10.1002/saj2.20068>, 2020.
- 802 Stein, O., Julien, P., Alonso, C.: Mechanics of jet scour downstream of a headcut, Journal of Hydraulic
803 Research, 31, 723–738, <https://doi.org/10.1080/00221689309498814>, 1993.
- 804 Su, Z.A., Xiong, D.H., Dong, Y.F., Zhang, B.J., Zhang, S., Zheng, X.Y., Fang, H.D.: Hydraulic properties
805 of concentrated flow of a bank gully in the dry - hot valley region of southwest China, Earth Surface
806 Processes and Landforms, 40, 1351 - 1363. <https://doi.org/10.1002/esp.3724>, 2015.
- 807 Su, Z.A., Xiong, D.H., Dong, Y.F., Li, J.J., Yang, D., Zhang, J.H., He, G.X.: Simulated headward erosion of
808 bank gullies in the Dry-hot Valley Region of southwest China, Geomorphology, 204, 532–541,
809 <https://doi.org/10.1016/j.geomorph.2013.08.033>, 2014.
- 810 Sun, W.Y., Mu, X.M., Song, X.Y., Wu, D., Cheng, A.F., Qiu, B.: Changes in extreme temperature and
811 precipitation events in the Loess Plateau (China) during 1960–2013 under global warming, Atmospheric
812 Research, 168, 33-48, <https://doi.org/10.1016/j.atmosres.2015.09.001>, 2016.
- 813 Thompson, J.R.: Quantitative effect of watershed variables on rate of gully - head advancement. Transactions
814 of the ASABE, 7, 54 - 55, <https://doi.org/10.13031/2013.40694>, 1964.
- 815 Torri, D., Poesen, J.: A review of topographic threshold conditions for gully head development in different
816 environments, Earth-Science Reviews, 130, 73–85, <https://doi.org/10.1016/j.earscirev.2013.12.006>, 2014.
- 817 Valentin, C., Poesen, J., Li, Y.: Gully erosion: Impacts, factors and control, Catena, 63, 132–153,
818 <https://doi.org/10.1016/j.catena.2005.06.001>, 2005.
- 819 Vandekerckhove, L., Poesen, J., Govers, G.: Medium-term gully headcut retreat rates in southeast Spain
820 determined from aerial photographs and ground measurements, Catena, 50(2-4), 329-352,
821 [https://doi.org/10.1016/S0341-8162\(02\)00132-7](https://doi.org/10.1016/S0341-8162(02)00132-7), 2003.
- 822 Vandekerckhove, L., Poesen, J., Wijdenes, D.O., Nachtergaele, J., Tomás de Figueiredo.: Thresholds for gully
823 initiation and sedimentation in Mediterranean Europe, Earth Surface Processes & Landforms, 25(11),
824 1201-1220, [https://doi.org/10.1002/1096-9837\(200010\)25:11<1201::AID-ESP131>3.0.CO;2-L](https://doi.org/10.1002/1096-9837(200010)25:11<1201::AID-ESP131>3.0.CO;2-L), 2015.
- 825 Vanmaercke, M., Poesen, J., Mele, B.V., Demuzere, M., Bruynseels, A., Golosov, V., Yermolaev, O.: How
826 fast do gully headcuts retreat?, Earth - Science Reviews, 154, 336 - 355,
827 <https://doi.org/10.1016/j.earscirev.2016.01.009>, 2016.
- 828 Vannoppen, W., Vanmaercke, M., De Baets, S., Poesen, J.: A review of the mechanical effects of plant roots on
829 concentrated flow erosion rates, Earth - Science Reviews, 150, 666 - 678,
830 <https://doi.org/10.1016/j.earscirev.2015.08.011>, 2015.
- 831 Vanwallegem, T., Bork, H.R., Poesen, J., Schmidtchen, G., Dotterweich, M., Nachtergaele, J., Bork, H.,
832 Deckers, J., Brüschen, B., Bungeneers, J., De Bie, M.: Rapid development and infilling of a buried gully under
833 cropland, Central Belgium, Catena, 63, 221–243, <https://doi.org/10.1016/j.catena.2005.06.005>, 2005.
- 834 Vanwallegem, T., Van Den Eeckhaut, M., Poesen, J., Deckers, J., Nachtergaele, J., Van Oost, K., Slenters, C.:
835 Characteristics and controlling factors of old gullies under forest in a temperate humid climate: a case study
836 from the Meerdaal Forest (Central Belgium), Geomorphology, 56(1), 15–29,
837 [https://doi.org/10.1016/S0169-555X\(03\)00043-6](https://doi.org/10.1016/S0169-555X(03)00043-6), 2003.



- 838 Wells, R.R., Alonso, C.V., Bennett, S.J.: Morphodynamics of Headcut Development and Soil Erosion in
839 Upland Concentrated Flows, *Soil Science Society of America Journal*, 73, 521–530.
840 <https://doi.org/10.2136/sssaj2008.0007>, 2009a.
- 841 Wells, R.R., Bennett, S.J., Alonso, C.V.: Effect of soil texture, tailwater height, and pore - water pressure on
842 the morphodynamics of migrating headcuts in upland concentrated flows, *Earth Surface Processes and*
843 *Landforms*, 34, 1867 – 1877, <https://doi.org/10.1002/esp.1871>, 2009b.
- 844 Wells, R.R., Momm, H.G., Rigby, J.R., Bennett, S.J., Bingner, R.L., Dabney, S.M.: An empirical investigation
845 of gully widening rates in upland concentrated flows, *Catena*, 101, 114–121,
846 <https://doi.org/10.1016/j.catena.2012.10.004>, 2013.
- 847 Wen, X., Wu, X., Gao, M.: Spatiotemporal variability of temperature and precipitation in Gansu province
848 (northwest China) during 1951–2015, *Atmospheric Research*, 197, 132–149,
849 <https://doi.org/10.1016/j.atmosres.2017.07.001>, 2017.
- 850 Wu, Bing., Wang, Zhanli., Zhang, Qingwei., Shen, Nan., Liu, June., Wang, Sha.: Evaluation of shear stress
851 and unit stream power to determine the sediment transport capacity of loess materials on different slopes,
852 *Journal of Soil & Sediments*, 18, 116–127, <https://doi.org/10.1007/s11368-017-1758-5>, 2018.
- 853 Wu, B., Wang, Z., Shen, N., Wang, S.: Modelling sediment transport capacity of rill flow for loess sediments
854 on steep slopes, *Catena*, 147, 453–462, <https://doi.org/10.1016/j.catena.2016.07.030>, 2016.
- 855 Xia, L., Song, X.Y., Fu, N., Li, H.Y., Li, Y.L.: Impacts of land use change and climate variation on green water
856 in the Loess Plateau Gully Region—A case study of Nanxiaohegou basin, *Journal of Hydraulic Engineering*,
857 48(6), 678–688, (In Chinese), 2017.
- 858 Xu, J.Z., Li, H., Liu, X.B., Hu, W., Yang, Q.N., Hao, Y.F., Zhen, H.C., Zhang, X.Y.: Gully Erosion Induced by
859 SnowmeUA in Northeast China: A Case Study, *Sustainability*, 11, <https://doi.org/10.3390/su11072088>, 2019.
- 860 Xu, X.M., Zheng, F.L., Wilson, G.V., Wu, M.: Upslope inflow, hillslope gradient and rainfall intensity impacts
861 on ephemeral gully erosion, *Land Degradation & Development*, 28, 2623–2635
862 <https://doi.org/10.1002/ldr.2825>, 2017.
- 863 Xu, X.M., Zheng, F.L., Qin, C., Wu, H.Y., Wilson, G.V.: Impact of cornstalk buffer strip on hillslope soil
864 erosion and its hydrodynamic understanding, *Catena*, 149, 417–425,
865 <https://doi.org/10.1016/j.catena.2016.10.016>, 2017.
- 866 Xu, X.M., Wang, H.B., Zhao, J.Y., Liu, X.J.: Dynamic variation of soil erosion of Nanxiaohegou small
867 watershed during 2004–2016, *Soil and Water Conservation in China*, 443(2), 59–61, (In Chinese), 2019.
- 868 Zhang, B.J., Xiong, D.H., Su, Z.A., Yang, D., Dong, Y.F., Xiao, L., Zhang, S., Shi, L.T.: Effects of initial step
869 height on the headcut erosion of bank gullies: a case study using a 3D photo-reconstruction method in the
870 Dry-hot Valley region of southwest China, *Physical Geography*, 37, 409–429,
871 <https://doi.org/10.1080/02723646.2016.1219939>, 2016.
- 872 Zhang, B.J., Xiong, D.H., Zhang G.H., Zhang, S., Wu, H., Yang, D., Xiao, L., Dong, Y.F., Su, Z.A., Lu, X.N.:
873 Impacts of headcut height on flow energy, sediment yield and surface landform during bank gully erosion
874 processes in the Yuanmou Dry - hot Valley region, southwest China, *Earth Surface Processes & Landforms*,
875 43(10), 2271–2282, <https://doi.org/10.1002/esp.4388>, 2018.
- 876 Zhang, H.X.: The characteristics of hard rain and its distribution over the Loess Plateau, *Acta Geographica*
877 *Sinica*, 38, 416–425, (In Chinese), 1983.



- 878 Zhang, G.H., Liu, Y.M., Han, Y.F., Zhang, X.C.: Sediment transport and soil detachment on steep slopes: I.
879 transport capacity estimation, *Soil Science Society of America Journal*, 73, 1291-1297,
880 <https://doi.org/10.2136/sssaj2008.0145>, 2009.
- 881 Zhao, A.C.: Analysis of control models of typical small watershed in gully area of Loess Plateau, the east part
882 of Gansu Province, *Research of Soil and Water Conservation*, 1, 45–49, (In Chinese), 1994.
- 883 Zhu, T.X.: Gully and tunnel erosion in the hilly Loess Plateau region, China, *Geomorphology*, 153, 144–155,
884 <https://doi.org/10.1016/j.geomorph.2012.02.019>, 2012.